Techno-Science

Scientific Journal of Mehmet Akif Ersoy University

www.dergipark.gov.tr/sjmakeu

Year	Volume	Issue
2018	1	1

Techno-Science

Scientific Journal of Mehmet Akif Ersoy University

www.dergipark.gov.tr/sjmakeu

Techno-Science

Scientific Journal of Mehmet Akif Ersoy University

Year: 2018 Volume: 1 Issue: 1

Scientific Journal of Mehmet Akif Ersoy University has been published three issues per year by Burdur Mehmet Akif Ersoy University.

Correspondence Address

Techno-Science
(Scientific Journal of Mehmet Akif Ersoy University)
Secetariat Office
Burdur Mehmet Akif Ersoy Üniversitesi
Bucak Teknoloji Fakültesi Dekanlığı
15300 Bucak / Burdur /Türkiye

Phone and e-mail
+90 248 325 99 00
techno-science@mehmetakif.edu.tr
techno-science@yandex.com

Printing

Burdur Mehmet Akif Ersoy Universitesi
Rektörlük Basım Merkezi
İstiklal Yerleşkesi
15030/Burdur/Türkiye

Phone
+90 248 213 10 00

Techno-Science

Scientific Journal of Mehmet Akif Ersoy University

Year: 2018 Volume: 1 Issue: 1

Techno-Science
Scientific Journal of Mehmet Akif Ersoy University

Preface to First Issue

Under the ownership of Burdur Mehmet Akif Ersoy University, Scientific Journal of Mehmet Akif Ersoy University (Techno-Science) has been published as of September-2018. Devotion and effort are required for a qualified academic journal. The DergiPark scholar journal management system has provided great convenience to control the processes of this journal. Of course there is a young, dynamic, original and hard-working team to control the processes of this journal. When everyone does their mission well, the management of all processes is perfect.

Techno-Science's editorial management on behalf of Burdur Mehmet Akif Ersoy University is Bucak Technology Faculty and Bucak Emin Gülmez Technical Sciences Vocational School is an important part of this management with its academic staff. Techno-Science will publish three issues a year. We believe that we have taken the first step successfully and we believe that there is a long way to go. We also know that our excitement for each number will increase exponentially.

Techno-Science will publish three numbers a year. We believe that we have taken the first step successfully and we believe that there is a long way to go. We also know that our excitement for each number will increase exponentially. We believe that in the very near future Techno-Science will be the shining star of Burdur Mehmet Akif Ersoy University. We would like to thank all the authors of their original papers for their efforts in the evaluation of these papers. It's about to meet the next issue.

September 30, 2018
Prof. Dr. Afşin GÜNGÖR
Executive Manager and Editor
On behalf of the Editorial Board

Techno-Science

Scientific Journal of Mehmet Akif Ersoy University

General Information

Scientific Journal of Mehmet Akif Ersoy University (Techno-Science) is a peer-reviewed, open access and refereed international journal published by Burdur Mehmet Akif Ersoy University. The first issue of the Techno-Science was published in 2018. Techno-Science accepts only English language manuscripts. Techno-Science publishes high quality original papers in the fields of engineering and sciences. The journal publishes research or review papers in the fields of applied science and technology such as Physics, Biology, Mathematics, Statistics, Chemistry and Chemical Engineering, Environmental Sciences and Engineering, Civil Engineering, Earth and Atmospheric Sciences, Electrical and Electronical Engineering, Computer Science and Informatics, Materials Sciences and Engineering, Mechanical Engineering, Mining Engineering, Industrial Engineering, Aeronautics and Astronautics, Architecture, Health Sciences, Pharmaceutical Sciences, and so on. It allows authors to submit articles online and track their progress via its web interface. The journal aims for a publication speed of 60 days from submission until final publication.

Article Processing Charge Policy

Techno-Science aims to publish extensive and reliable information on current developments, innovative technologies and discoveries about science and technology. Papers will be freely accessible online without any subscriptions and restrictions to researchers worldwide. The journal doesn't have Article Processing Charge (APC) or any submission charges.

Plagiarism Policy

Scientific Journal of Mehmet Akif Ersoy University does not use a plagiarism checker tool currently. However, if a plagiarism is detected during reviewing or editing stages before publication, authors have to rewrite the relevant sections of the manuscript. If an extensive plagiarism is detected the manuscript may be rejected directly. If a plagiarism is detected after publication process of the paper, editor will inform the author's institute and funding services. The relevant sections of the paper will be marked on the article.

Copyright Policy

The authors of the articles published in Techno-Science retain the copyright of their publications. Authors are free to reproduce and disseminate their work. Aurhors can use all or part of their article in compilations or other publications of their own work.

Techno-Science
Scientific Journal of Mehmet Akif Ersoy University

Author Guidelines

All manuscripts must be in English. Pages should be numbered sequentially. The maximum length of contributions is 10 pages (short manuscripts should be less than 4 pages). Longer contributions will only be accepted if authors provide justification in a cover letter which must be added at submission as a supplementary file.

Please add a cover letter as a supplementary file stating the following information about the submitted paper:

1. Paper title, list of authors
2. The type of your paper: original scientific paper, review scientific paper, or short scientific paper.
3. A declaration that your paper is unpublished work, not considered elsewhere for publication.
4. State the value of the paper or its practical, theoretical and scientific implications. What is new in the paper with respect to the state-of-the-art in the published papers?
5. We kindly ask you to suggest at least two reviewers for your paper and give us their names and contact information (email).

Every manuscript submitted to the Techno-Science undergoes the course of the peer-review process.

THE FORMAT OF THE MANUSCRIPT

The manuscript should be written in the following format:

- A title, which adequately describes the content of the manuscript.
- An Abstract should not exceed 250 words. The Abstract should state the principal objectives and the scope of the investigation, as well as the methodology employed. It should summarize the results and state the principal conclusions.
- 4-6 significant key words should follow the abstract to aid indexing.
- An Introduction, which should provide a review of recent literature and sufficient background information to allow the results of the article to be understood and evaluated.
- A Theory or experimental methods used.
- An Experimental section, which should provide details of the experimental set-up and the methods used for obtaining the results.
- A Results section, which should clearly and concisely present the data using figures and tables where appropriate.
- A Discussion section, which should describe the relationships and generalizations shown by the results and discuss the significance of the results making comparisons with previously published work. (It may be appropriate to combine the Results and Discussion sections into a single section to improve the clarity).
- Conclusions, which should present one or more conclusions that have been drawn from the results and subsequent discussion and do not duplicate the Abstract.
- References, which must be cited consecutively in the text using square brackets [1] and collected together in a reference list at the end of the manuscript.

Units standard SI symbols and abbreviations should be used. Symbols for physical quantities in the text should be written in italics (e.g. *v*, *T*, *n*, etc.). Symbols for units that consist of letters should be inplain text (e.g. ms^{-1}, K, min, mm, etc.).

Abbreviations should be spelt out in full on first appearance, e.g., variable time geometry (VTG). Meaning of symbols and units belonging to symbols should be explained in each case or quoted in a special table at the end of the manuscript before References

Figures must be cited in a consecutive numerical order in the text and referred to in both the text and the caption as Fig. 1, Fig. 2, etc. Figures should be prepared without borders and on white grounding and should be sent separately in their original formats.

Pictures may be saved in resolution good enough for printing in any common format, e.g. BMP, GIF or JPG. However, graphs and line drawings should be prepared as vector images, e.g. CDR, AI. When labeling axes, physical quantities, e.g. t, v, m, etc. should be used whenever possible to minimize the need to label the axes in two languages. Multicurve graphs should have individual curves marked with a symbol. The meaning of the symbol should be explained in the figure caption.

Tables should carry separate titles and must be numbered in consecutive numerical order in the text and referred to in both the text and the caption as Table 1, Table 2, etc. In addition to the physical quantity, e.g. t (in italics), units (normal text), should be added in Strojniški vestnik - Journal of Mechanical Engineering 2 square brackets. The tables should each have a heading. Tables should not duplicate data found elsewhere in the manuscript.

Acknowledgement of collaboration or preparation assistance may be included before References. Please note the source of funding for the research.

REFERENCES

A reference list must be included using the following information as a guide. Only cited text references are included. Each reference is referred to in the text by a number enclosed in a square bracket (i.e., [3] or [2] to [6] for more references). No reference to the author is necessary.

References must be numbered and ordered according to where they are first mentioned in the paper, not alphabetically. All references must be complete and accurate. All non-English or. non-German titles must be translated into English with the added note (in language) at the end of reference. Examples follow.

Journal Papers:
Surname 1, Initials, Surname 2, Initials (year). Title. *Journal*, volume, number, pages, DOI code. Journal titles should not be abbreviated. Note that *Journal Title* is set in italics.

[1]. Gungor, A. (2010). Simulation of emission performance and combustion efficiency in biomass fired circulating fluidized bed combustors. *Biomass and Bioenergy* vol. 34, no. 4 p. 506-514, DOI: 10.1016/j.biombioe.2009.12.016.

Books:
Surname 1, Initials, Surname 2, Initials (year). Title. Publisher, place of publication. Note that the *Title of the Book* is italicized.

[2]. Groover, M.P. (2007). *Fundamentals of Modern Manufacturing.* John Wiley & Sons, Hoboken.

Chapters in Books:
Surname 1, Initials, Surname 2, Initials (year). Chapter title. Editor Surname 1, Initials, Editor Surname 2, Initials (ed(s).), *Book title.* Publisher, place of publication, pages. Note that the *Book title* is italicized.

[3]. Carbone, G., Ceccarelli, M. (2005). Legged robotic systems. Kordić, V., Lazinica, A., Merdan, M. (eds.), *Cutting Edge Robotics*. Pro literatur Verlag, Mammendorf, p. 553-576.

Proceedings Papers:
Surname 1, Initials, Surname 2, Initials (year). Paper title. Proceedings title, pages. Note that the *Proceedings Title* is italicized.

[4]. Li R.T.H., Chung S.H. (2008). Digital boundary controller for single-phase grid-connected CSI. *IEEE 2008 Power Electronics Specialists Conference,* p. 4562-4568.

Standards:
Standard-Code (year). Title. Organisation. Place. Note that the *Title of the Standard* is italicized.

[5]. BS EN 14214:2012+A1:2014. *Liquid petroleum products - Fatty acid methyl esters (FAME) for use in diesel engines and heating applications - Requirements and test methods.* The British Standards Institution. London.

Patents
Standard-Code (year). Title. Organisation. Place. Note that the *Title of the Standard* is italicized.

Surname 1, Initials, Surname 2, Initials (year). *Patent No.* Place of publication: Publisher. Note that *Patent no.* is set in italics.

[6]. Tsukahara, E., Takurou, K. (2015). *U.S. Patent No. 9010288*. Shizuoka: U.S. Patent and Trademark Office.

www pages:
Surname, Initials or Company name. Title, from *http://address,* date of access. Note that the *www address* is italicized.

[7]. Mehmet Akif Ersoy University, from *http://www.mehmetakif.edu.tr*, accessed on 2018-05-01.

Reports:
Surname 1, Initials, Surname 2, Initials (year). *Title of the Report* (Report No: XXX). Place of Publication: Publisher. Note that *Title of the Report* is set in italics.

[8]. Yager, J. (2000). *Practice guidelines for the treatment of patients with eating disorders* (2nd ed.). Washington, DC: American Psychiatric Association.

EXTENDED ABSTRACT (SHORT SCIENTIFIC PAPER)

By the time the paper is accepted for publishing, the authors are requested to send the extended abstract (approx. one A4 page or 3.500 to 4.000 characters).

COPYRIGHT

Along the submission file of the manuscript authors will add a cover letter as a supplementary file. All accepted manuscripts must be accompanied by a Copyright Transfer Agreement, which should be sent to the editor. Authors submitting a manuscript do so on the understanding that the work has not been published before, is not being considered for publication elsewhere and has been read and approved by all authors. The work should be original by the authors and not be published elsewhere in any language without the written consent of the publisher.

The proof will be sent to the author showing the final layout of the article. Proof correction must be minimal and fast. Thus it is essential that manuscripts are accurate when submitted.

Authors can track the status of their articles on web site on DergiPark of the Techno-Science

ARTICLE PROCESSING CHARGE (APC)

The journal doesn't have Article Processing Charge (APC) or any submission charges.

DIGITAL DATA REQUIREMENT

Main article submission file should be in editable data format, preferably .doc/.docx. The size of the document should not exceed 10 MB, if it does, the upload process will NOT be successful. Large size of the document is usually due to the size of figures, so we suggest you save them under smaller resolution in article file and upload original figures as supplementary file.

Due to a large number of papers that are submitted, we only consider reviewing submissions that are in accordance with the guidelines above.

CORRESPONDENCE ADDRESS

Address : Techno-Science (Scientific Journal of Mehmet Akif Ersoy University)
Secetariat Office
Burdur Mehmet Akif Ersoy Üniversitesi
Bucak Teknoloji Fakültesi Dekanlığı
15300 Bucak / Burdur /Türkiye
Phone : +90 248 325 99 00
e-mail : techno-science@mehmetakif.edu.tr

This page intentionally left blank

Techno-Science

Scientific Journal of Mehmet Akif Ersoy University

Year: 2018 Volume: 1 Issue: 1

CONTENTS

Techno-Science *Issue ID: 39235*

This page intentionally left blank

Techno-Science

Scientific Journal of Mehmet Akif Ersoy University

www.dergipark.gov.tr/sjmakeu

INVESTIGATION OF COMBINED EFFECT OF NANOFLUID AND SWIRLING JET ON HEAT TRANSFER

Mustafa KILIÇ[1*]

[1] *Department of Mechanical Engineering, Adana Science and Technology University, Adana, Turkey*

ARTICLE INFO

Article History

Received : 17/08/2018
Revised : 19/09/2018
Accepted : 19/09/2018
Available online : 30/09/2018

Keywords

Computational Fluid Dynamics
Heat Transfer
Nanofluid
Swirling Jet

ABSTRACT

The present study is focused on the numerical investigation of heat transfer from a heated surface by using nanofluids and swirling jets. Effects of different Reynolds number and different inlet temperature on heat transfer and fluid flow were studied numerically. Al_2O_3-H_2O nanofluid was used as a base coolant in all parameters. k-ω turbulent model of PHOENICS computational fluid dynamics code was used for numerical analysis. It is obtained that increasing Reynolds number from Re=12000 to 21000 causes an increase of 51.3% on average Nusselt Number. Increasing inlet temperature from T_{inlet}=5°C to 30°C has not a significant effect on average Nusselt number.

1. INTRODUCTION

One of the main problems of design parameter for new technological devices are heat loads. Using swirling flow with nanofluids can be a key solution to solve this heat loads problem. So, swirling flows have gained an increasing interest in the last decade in fluid dynamics research, since in many technical applications swirl is an essential phenomenon. Swirling flows are generally used in the industry for separation, mixing and flame stabilization. The main characteristic of swirling flow is the combination of axial and tangential velocities. Swirling flows are used to minimize pressure drop and prevent particle deposition (Kharoua et al.[1]). In swirling flows, part of the fluid enters axially while the remainder is injected tangentially at various locations along the tube axis. The radial pressure gradient results in thinning of thermal boundary later with an accompanying improvement in heta transfer (Chang et al. [2]). A nanofluid is defined as a suspension of solid particles which have 1-100 nm size in a base fluid. In heat transfer applications using nanofluid, the particles suspended in the base fluid, expand thermal capacity of the fluid. Interactions and collisions between particles cause to increase in turbulence and turbulence intensity of the transition surface. Turbulence intensity and large surface area enables more heat transfer. Nanoparticles carry 20% of their atoms at the surface that makes them ready to heat transfer. Another advantage of using nanofluids is the particle agitation cause micro-convection in the fluid due to its very small size and therefore increases the heat transfer in particular heat transfer from surfaces with high heat flux, as well as industry, medicine and space research. But main disadvanteges of using nanofluid may be pressure drop an particle deposition in pipes or ducts. So using nanofuids with swirling jets may be a key solution for these disadvanteges.

Many studies on enhancing heat transfer technique as impinging jets or swirling jets with different coolant can be found in the literature. Kilic et al. [3, 4] surveyed the cooling of a flat plate with the support of the impinging fluid air jet for different Reynolds numbers and dimensionless channel heights. The average Nusselt number was found to increase by 49.5% in Re = 4000-10000 and 17.9% in H/D_h = 4-10. Teamah et al. [5] investigated heat transfer and flow structure formed by Al_2O_3 nanofluid to flat plate by experimentally and numerically with various Re number (Re=3000-32000) and different volume ratio of nanofluids (φ=0-10%). As the nanoparticles in the base fluid increases, the heat transfer from the surface increases and heat transfer coefficient can be enhanced by 62% according to the

* Corresponding Author: mkilic@adanabtu.edu.tr

To cite this article: Kilic, M. (2018). Investigation of combined effect of nanofluid and swirling jet on heat transfer. *Techno-Science* vol. 1, no. 1 p. 1-5.

water is used base fluid only. They observed that heat transfer can be increased of 8.9% by using CuO-water with respect to Al_2O_3-water. Sun et al. [6] researched the effect of a single impinging jet using Cu-water nanofluids as working fluid on heat transfer. It has been determined that when the nanofluid is used, important enhancement can be achieved in heat transfer with respect to the use of water only, no significant change in pressure drop, a higher heat transfer coefficient is obtained when a circular nozzle is used, and a higher heat transfer coefficient is obtained when the jet angle is 90°. Kilic et al. [7] investigated the heat transfer from a high heat flux surfaces for different parameters using nanofluids and multiple impinging jets. It was found that increase on Re number and decrease on particle diameter causes an increase on heat transfer. The use of Cu-water nanofluid causes an increase of 9.3% and 8.4% on heat transfer according to the use of Al_2O_3-water and TiO-water nanofluid.Sekrani et al. [8] investigated turbulent convective heat transfer of Al_2O_3 nanofluid flowing in a circular tube with uniform heat flux for different turbulenc model numerically. Their results show that SST k-ω model perfoms best for predicting average Nusselt number and friction factor according to the other turbulence models. Wongcharee et al. [9] investigated effects of swirling impinging jets with TiO_2-water nanofluid on heat transfer for different jet-to-target speacing ratio, Reynolds number and volume consantration. Their results show that increasing volume ratio up to the 2% causes an increase on average Nusselt number but while the one with concentration of 2.5% shows opposite results. Akyurek et al. [10] studied on turbulent forced convection heat transfer and pressure drop characteristic of Al_2O_3-water nanofluid experimentally by using wire coil turbulators. They obtained that average Nusselt number increases with increasing the Reynolds number and particle concentration. The pressure drop of the Al_2O_3-water nanofluid showed neqarly equal to that of oure water at the same Reynolds number rage. Using wire coil turbulators increase pressure drop as well as the heat transfer coefficient.

This study is different from the studies at literature by evaluating combined effect of swirling jets and nanofluids on heat transfer for different parameters to prevent the disadvanteges (pressure drop and particle deposition) of nanofluids. By using combined effect of nanofluids and swirling flows heat transfer enhancement was evaluated for different Reynolds number and different inlet temperature. Numerical results was also validated with the experimental results in literature.

2. NUMERICAL MODEL

Compuatitional domain consists of a rectangular channel of which dimensions are 10x10x50 mm. Two jet inlets of which dimensions are 3x3 mm were located at inverse direction to inject tangentially. There is one outlet at the end of the channel. All walls has a constant wall temperature. Inlet velocity of swirling jets are applied according to the Reynolds number. Inlet temperature of fluid is changed according to the different inlet temperature. k-ω turbulence model of PHOENICS CFD code was used for this numerical analysis. CFD simulation domain is shown in Fig.1 and mesh structure is shown in Fig.2.

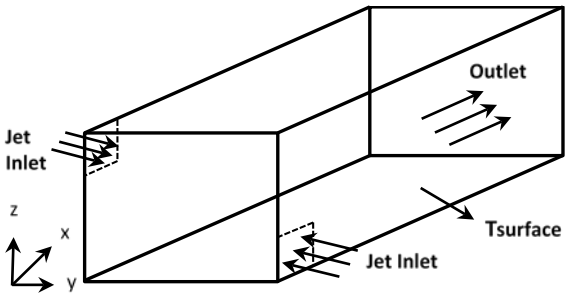

Fig.1. *CFD Simulation model*

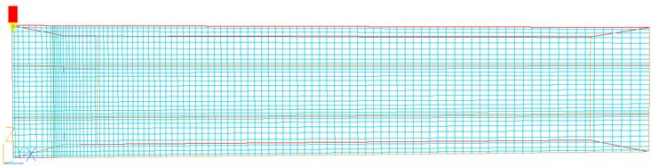

Fig.2. *Mesh Structure*

The continuity, Reynolds averaged momentum and time averaged energy equations governing 3-dimensional steady, flow of fluid with constant properties used for turbulent solutions can be written in the Cartesian coordinate system as follows;

Continuity equation:

$$\frac{\partial U_i}{\partial x_i} = 0 \tag{1}$$

Momentum equation:

$$\rho U_i \frac{\partial U_j}{\partial x_i} = -\frac{\partial P}{\partial x_j} + \frac{\partial}{\partial x_i}\left[\mu\left(\frac{\partial U_i}{\partial x_j} + \frac{\partial U_j}{\partial x_i}\right) - \rho\overline{u_i' u_j'}\right] \tag{2}$$

Energy equation:

$$\rho c_P U_i \frac{\partial T}{\partial x_i} = \frac{\partial}{\partial x_i}\left[k\frac{\partial T}{\partial x_i} - \rho c_P \overline{u_i' T'}\right] \tag{3}$$

where Uτ is the resultant fricon velocity ($U\tau = \sqrt{(\tau_w/\rho)}$, τ_w is the wall shear stress, δ is the normal distance of the first grid point from the wall, and k is von Karman's constant. Aditionally, Vinlet is the bulk inlet velocity, I is the turbulent intensity (typically in the range $0.01<I<0.05$), ε is the dissipaon rate, C_d is the constant (C_d=0.09) and the mixing length $L_m \sim 0.1H$, where H is a characterisc inlet dimension.

Table 1. *Boundary Conditions*

	U (m/s)	V (m/s)	W (m/s)	T °C	k	ω
Inlet	$U=0$	$V=V_{inlet}$	$W=0$	$T=T_{inlet}$	$k=(I\cdot V_{inlet})$	$\omega=\varepsilon/(C_d\cdot k)$
Outlet	$\partial U/\partial x=0$	$\partial U/\partial y=0$	$\partial U/\partial z=0$	$T=T_{outlet}$	$\partial k/\partial z=0$	$\partial\omega/\partial z=0$
Bottom Wall	$U=0$	$V=0$	$W=0$	$T=T_{surface}$	$k=U\tau^2/\sqrt{C_d}$	$\omega=U\tau/(\sqrt{C_d}\kappa\delta)$
Top Wall	$U=0$	$V=0$	$W=0$	$T=T_{surface}$	$k=U\tau^2/\sqrt{C_d}$	$\omega=U\tau/(\sqrt{C_d}\kappa\delta)$
Front and Backwall	$U=0$	$V=0$	$W=0$	$T=T_{surface}$	$k=U\tau^2/\sqrt{C_d}$	$\omega=U\tau/(\sqrt{C_d}\kappa\delta)$

3. DATA REDUCTION

The heat transfer from the surfaces to the fluid will take place by convection, conduction and radiation.

$$\dot{Q}_{convection}=\dot{Q}_{total}-\dot{Q}_{conduction}-\dot{Q}_{radiaiton} \quad (4)$$

Heat transfer occurs from high temperature walls to the nanaofluid. So heat transfer rate gained by nanaofluid equals to the heat transfer rate lost by walls. As a result, walls surfaces will be cooled by using nanofluid with swirling jet. It is assume that channel walls has constant temperature. So heat conduction through the walls (from outer surface to the inner surface) is neglected. Heat transfer with radiation is negligible in this study because surface temperature is under 573.15 K.

Heat transfer rate gained by the fluid from wall surfaces;

$$\dot{Q}=\dot{m}C_{p_{nf}}(T_{outlet}-T_{inlet}) \quad (5)$$

Where $\dot{m}$ is mass flow rate of nanaofluid, $C_{P_{nf.}}$ is nanaofluid specific heat, T_{outlet} is outlet temperature of nanaofluid and T_{inlet} is inlet temperature of nanofluid. Nusselt number (Nu) is a dimensionless parameter indicating the ratio of heat transfer with convection to heat transfer with conduction. Averaege Nusselt number can be presented as ratio of average heat transfer coefficient times characteristic length (D_h) to the coefficient of thermal conductivity of the nanofluid.

$$Nu_{avg}=\frac{h_{avg}\cdot D_h}{k_{nf}} \quad (6)$$

Where h_{avg} is the average heat transfer coefficient, measured, D_h is the hydraulic diameter, and k_{nf} is the coefficient of thermal conductivity of the nanofluid. Averaege heat transfer coefficient can be presented as;

$$h_{avg}=\dot{Q}/(A_s.T_{lm}) \quad (7)$$

Where A_s is the convection surface area and T_{lm} is logarithmic mean temperature of nanaofluid.

$$T_{lm}=(\Delta T_e-\Delta T_i)/\ln\left(\frac{\Delta T_e}{\Delta T_i}\right) \quad (8)$$

Where ΔT_e is temperature difference between surface temperature and nanaofluid exit temperature $\Delta T_e=(T_s-T_e)$ and ΔT_i is temperature difference between surface temperature and nanaofluid inlet temperature $(\Delta T_i=(T_s-T_i)$. Reynolds number (Re) is used to determine for forced convection whether the flow is laminar or turbulent. Reynolds number based on turbulent flow;

$$Re=\frac{\rho_{nf}V_{jet}D_h}{\mu_{nf}} \quad (9)$$

Where ρ_{nf} is the nanofluid density, V_{jet} is the jet velocity, and μ_{nf} is the nanofluid dynamic viscosity. The density of nanofluids is;

$$\rho_{nf}=(1-\varphi)\rho_{bf}+\varphi\rho_p \quad (10)$$

Where ρ_{bf} is the base fluid (water) density, φ is the volumetric ratio of the nanofluid, and ρ_p is the density of the solid particles in the nanofluid. The volumetric ratio of nanoparticles is;

$$\varphi=\frac{1}{(1/\omega)(\rho_p-\rho_{bf})} \quad (11)$$

Where ω is the density difference between the fluid and the main fluid (water). The nanofluid specific heat is calculated from;

$$C_{p_{nf}}=\frac{\varphi(\rho C_p)_p+(1-\varphi)(\rho C_P)_f}{\rho_{nf}} \quad (12)$$

Where $(C_p)_p$ is specific heat of particle $(C_p)_p$ is specific heat of base fluid. The effective thermal conductivity of nanofluid is calculated according to Corcione [11];

$$\frac{k_{eff}}{k_f}=1+4.4Re^{0.4}Pr^{0.66}\left(\frac{T_{nf}}{T_{fr}}\right)^{10}\left(\frac{k_p}{k_f}\right)^{0.03}\varphi^{0.66} \quad (13)$$

Where Re is the nanoparticle Reynolds number, Pr is the Prandtl number of the base liquid. k_p is the nanoparticle thermal conductivity, φ is the volume ratio of the suspended nanoparticles, T_{nf} is the nanofluid temperature (K), T_{fr} is the freezing point of the base liquid. Nanoparticle Reynolds number is defined as;

$$Re=\frac{2\rho k_b fT}{\pi\mu f^2 d_p} \quad (14)$$

k_b is the Boltzmann's constant. The effective dynamic viscosity of nanofluids defined as;

$$\mu_{nf} = \mu_{bf}(1 + 2.5\varphi + 4.698\varphi^2) \quad (15)$$

4. RESULTS AND DISCUSSIONS

In this section, numerical results were prepared for two parameters. Effects of Al_2O_3-water nanofluid with 20 nm particle diameter and volume ratio of φ=4% on heat transfer for different Reynolds number (Re=12000, 15000, 18000, 21000) and for different inlet temperature (T_{inlet} =5, 10, 20, 30°C) were obtained.

4.1. Effects of different Reynolds number on heat transfer

To understand effect of fluid velocity on heat transfer, Reynolds number was increased from Re=12000 to 21000. Fig.3 and Fig.4 show velocity vector and temperature contours of fluid flow at the midpoint of inlet of swirling jet, in the middle of channel and outlet of the channel at x-direction (x/D_h=0.03, 8, 16) for Re=12000 and 21000 respectively.

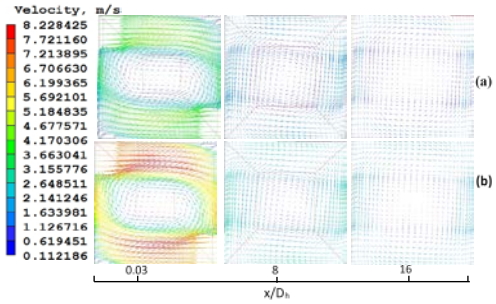

Fig.3. *Velocity vectors for different Reynolds Number (a) Re=12000 and (b) Re= 21000*

Thermal boundary region does not occure at the inlet of swirling jet because of the high turbulence intensity at the surfaces of the channel. Temperature increase can be seen only at the impinging region of swirling jet because fluid velocity decreases at these region. Velocity vectory occurs in a shape of flattened sphere. So effect of swirling jet can be seen significantly at the inlet region fo swirling jets. At the middle of the channel thermal boundary layer is thickening because of the velocity decrease (decrease of hydrodynamic boundary layer) at the corner of the rectangular channel.

This boundary layer thickness increase can be seen at the direction of swirling flow. Because separation of fluid flow is more evident at these region. At the end of the channel, decrease of fluid velocity can be seen easily. Seperation of the fluid flow is more important at the corner of the channel at this region. Decreasing hydrodynamic boundary layer thickness causes an increase on thermal boundary layer thickness and it causes an increase on surface temperature. So increasing Reynolds number causes an increase on hydrodynamic boundary layer and decrease on themal boundary layer and surface temperature. Variation of average Nusselt number for different Reynolds number is shown in Fig.5.

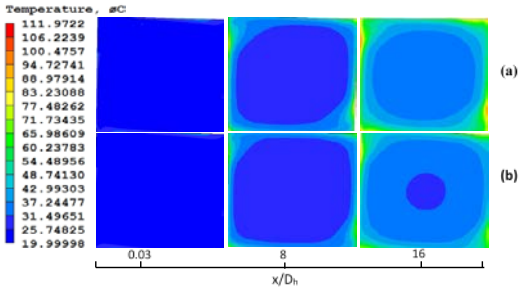

Fig.4. *Temperature contours for different Reynolds Number (a) Re=12000 and (b) Re= 21000*

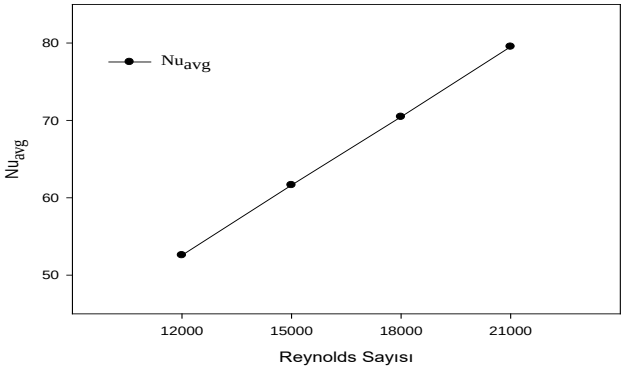

Fig.5. *Average Nusselt Number of Al_2O_3-H_2O nanofluid for different Reynolds Number*

It is obtained that increasing Reynolds number causes an increase on average Nusselt number and decrease on surface temperature. So increasing Reynolds number from Re=12000 to 21000 causes an increase of 51.3% on average Nusselt Number. But this increase decreases gradually. Increasing Reynolds number from Re=12000 to 15000 causes an increase of 17.2% on average Nusselt number. But this increase decreases to 14.3% and 12.9% for Reynolds number increase from Re=15000 to 18000 and Re=18000 to 21000.

4.2. Effects of Different Inlet Temperature on Heat Transfer

Fig.6 shows average Nusselt number for different inlet temperature (T_{inlet}= 5, 10, 20, 30°C) of Al_2O_3-H_2O when it is used at 20 nm particle size and φ=4% at Re=18000. It can be seen that increasing inlet temperature has not a considerable effect on average Nusselt number. The reason of this is increasing or decreasing the inlet temperature causes a change on heat convection coefficient.

This means that heat flux from the surface to the fluid changes temperature difference between bulk fluid temperature and avarege surface temperature. So surface temperature can be change but it does not cause a significant change on average Nusselt number. Temperature contours for different inlet temperature are shown in Fig.7.

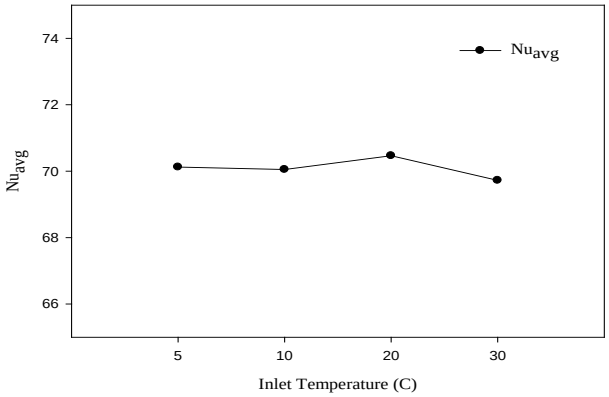

Fig. 6. *Average Nusselt numbers of Al_2O_3-H_2O nanofluid for different inlet temperature*

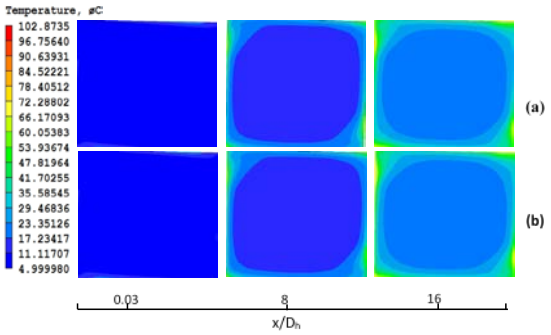

Fig.7. *Temperature contours of Al_2O_3-H_2O nanofluid for different inlet temperature (a) T_{inlet}= 5ºC and (b) T_{inlet}= 30ºC*

5. CONCLUSIONS

The present study is focused on the numerical investigation of heat transfer from a heated surface by using nanofluids and swirling jets. Effects of different Reynolds number, different inlet temperature on heat transfer and fluid flow were studied numerically. It is obtained that increasing Reynolds number from *Re*=12000 to 21000 causes an increase of 51.3% on average Nusselt Number. Increasing inlet temperature from T_{inlet}=5ºC to 30ºC has not a significant effect on average Nusselt number. Difference between numerical results of this study and experimental results is less than 11% for *Re*=12000-18000. Research areas for future investigations can be using different particle diameter, different volume ratio and different types of nanofluids with different application geometries and cooling techniques to obtain combined effect of nanofluid and swirling jets.

ACKNOWLEDGEMENTS

The financial support of this study by Scientific Research Projects (18103006 and 1610321) of Adana Science and Technology University is gratefully acknowledged.

REFERENCES

[1]. Kharoua, N., Khezzar L., Alshehhi M., (2018). The interaction of confined swirling flow with conical bluff body: numerical simulation. Chemical engineering research and design, vol.136, p .207-218.

[2]. Chang F., Dhir VK., (1993). Heat transfer enhancement and turbulent flow field in tangentially injected swirl flows in tubes. American Society of Mechanical Engineers Heat Transfer Division, vol. 256, p.37-48.

[3]. Kilic, M., Calisir, T., Baskaya, S., (2017). Experimental and numerical study of heat transfer from a heated flat plate in a rectangular channel with an impinging Jet, Journal of the Brazilian Society of Mechanical Sciences and Engineering. vol.39, 1, p.329-344.

[4]. Kilic, M., Baskaya, S., (2017). Improvement of heat transfer from high heat flux surfaces by using vortex promoters with different geometries and impinging jets. Journal of the Faculty of Engineering and Architecture of Gazi University, vol.32 number (3), p.693-707.

[5]. Teamah, M. A., Dawood, M.M., Shehata, (2016). A Numerical and experimental investigation of flow structure and behavior of nanofluids flow impingement on horizontal flat plate, Experimental Thermal and Fluid Science, vol.74, p. 235-246.

[6]. Sun, B., Qu, Y., Yang, D., (2016). Heat transfer of Single Impinging jet with Cu nanofluids, Applied Thermal Engineering, vol.102 p.701-707.

[7]. Kilic, M., Ali H.M., (2018). Numerical investigation of combined effect of nanofluids and multiple impinging jets on heat transfer, Thermal Science, , DOI:10.2298/TSCI171204094K.

[8]. Sekrani, G., Poncet, S., Proulx, P., (2018). Modelling of convective turbulent heat transfer of water-based Al2O3 nanofluids in an uniformly heated pipe, Chemical Engineering Science, vol.176, p.205-219.

[9]. Wongcharee, K., Chuwattanakul, v., Eiamsa-ard, S., (2017). Heat transfer of swirling impinging jets with TiO2-water nanofluids, Chemical Engineering and Porcessing, vol.114, p.16-23.

[10]. Akyurek, E.F., Geliş, K., Şahin, B., Manay, E., (2018). Experimental Anlaysis of nanaofluid with wire coil turbulators in a concentric tube heat exchanger, Results in Physics,vol. 9, p. 376-389.

[11]. Corcione, M., (2011). Empirical correlating quations for predicting the effective thermal conductivity and dynamic viscosity of nanofluids, Energy Conversation Management, vol. 52, number.1, p.789-93.

Techno-Science

Scientific Journal of Mehmet Akif Ersoy University

www.dergipark.gov.tr/sjmakeu

EFFECT OF MEAN PISTON SPEED AND RESIDUAL GAS FRACTION ON PERFORMANCE OF A FOUR-STROKE IRREVERSIBLE OTTO CYCLE ENGINE

Abdullah Onur ÖZDEMİR[1], Bayram KILIÇ[2], Emre ARABACI[2], Recep Çağrı ORMAN[3]*

[1] *Department of Automotive Engineering, Technology Faculty, Gazi University, Ankara, Turkey*
[2] *Department of Automotive Technology, Bucak Emin Gülmez Vocational School, Burdur Mehmet Akif Ersoy University, Burdur, Turkey*
[3] *Department of Automotive Technology, Tusaş Kazan Vocational School, Gazi University, Ankara, Turkey*

HIGHLIGHTS

- The irreversible Otto cycle was modeled with the finite-time thermodynamics.
- The performance of the irreversible Otto cycle was investigated in terms of mean piston speed and residual gas fraction.
- The results obtained are reference of the engine designers.

GRAPHICAL ABSTRACT

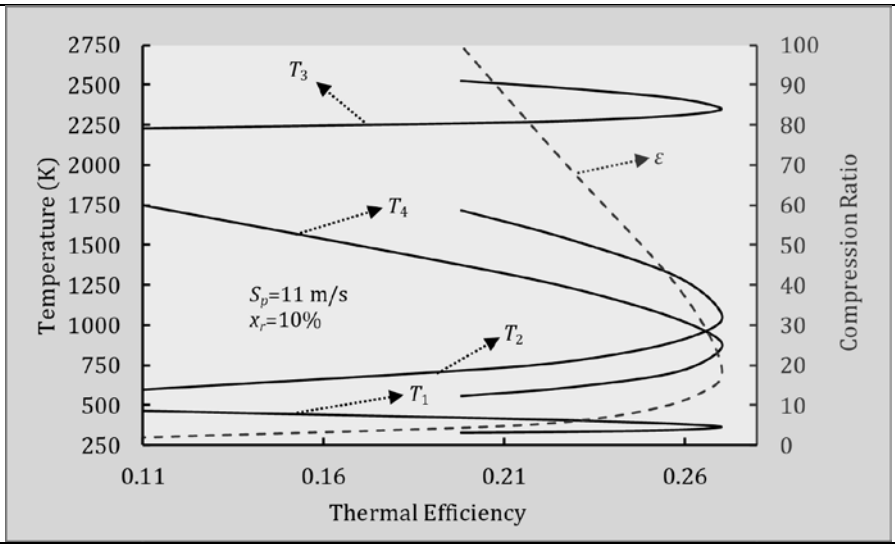

ARTICLE INFO

Article History

Received	:	20/08/2018
Revised	:	19/09/2018
Accepted	:	19/09/2018
Available online	:	30/09/2018

Keywords
Otto cycle modeling
Performance
Mean piston speed
Residual gas fraction

ABSTRACT

In this study, a four-stroke irreversible Otto cycle model was constructed using the finite time thermodynamics to investigate the effect of the mean piston speed and the residual gas fraction on the cycle (or engine) performance. Fuel consumption was taken as a function of mean piston speed, and initial cycle temperature was considered as a function of residual gas fraction. It has been assumed that the specific heat does not change depending on the temperature. A detailed numerical example study has been made to see the effect of the mean piston speed and the residual gas fraction on engine performance. As a result of the numerical example made, the cycle thermal efficiency and the dimensionless power output were observed with the increase of the residual gas amount and the mean piston speed. We think that the results obtained are especially important for engine designers.

1. INTRODUCTION

Otto cycle heat engines are widely used in many areas, from industrial to transportation, and are the main power source for many modern machines such as automobiles, agricultural machines, transport vehicles and generators [1]. By using thermodynamics to analyze the performance of the Otto cycle heat engine, the rules for the development

* Corresponding Author: recepcagriorman@gmail.com

To cite this article: Özdemir, A.O., Kılıç, B., Arabacı, E., Orman, R.Ç. (2018). Effect of mean piston speed and residual gas fraction on performance of a four-stroke irreversible Otto cycle engine. *Techno-Science* vol. 1, no. 1 p. 6-12.

and use of novel technologies can be determined or can be developed to optimize the Otto cycle engine. Using classical thermodynamics to conduct the first law analysis for the Otto cycle, one can examine the quantitative relationship between efficiency and different losses [2]. Using the second law of thermodynamics to analyze the performance of the Otto cycle, loss of work capacity due to various irreversible losses in the energy conversion process can be investigated [3]. In order to analyze the performance of the Otto cycle it is possible to obtain more realistic results with the finite-time thermodynamics taking into account the irreversibilities in addition to the first law of thermodynamics. [4].

As a novel branch of modern thermodynamic theory, finite time thermodynamics (FTT) has made great progress in recent years. FTT has also been applied to performance analysis, optimization and optimal configuration studies for internal combustion engine cycles [5].

In modern thermodynamic theories it is important to use FTT to analyze and optimize the performance of real thermodynamic cycles and processes. The fundamental problem of FTT can be divided into two cases: research on optimum performance for a given thermodynamic process and on optimal configuration for a thermodynamic process when optimization objectives are given [6-9].

The researches on optimal performances of Otto cycle include the following three aspects: the optimal performance with con-stant specific heats; the optimal performance with variable specific heats; the optimal performance with variable specific heat ratio [5].

There are many studies in the literature about the analysis of the otto cycle with FTT. Wu et al. investigated the effect of combustion on irreversible Otto cycle performance and derived the relationship between maximum work output and optimum compression ratio at maximum operating temperature [10-12]. Chen et al., irreversible Otto cycle, relate the cycle between work and utility, and the relationship between the initial temperature and heat transfer is derived [13]. Hou evaluated irreversible Otto cycle and Atkinson cycles in terms of maximum work output and thermal efficiency [14]. Ge et al. have investigated the effects of specific heat changes on irreversible Otto cycle performance [1]. Ge et al. have built a model for the irreversible Otto cycle with air standard acceptance of internal irreversibilities, frictional losses and heat transfer losses accounted for, and analyzed cycle performance with the entropy generation rate and ecological function parameters for the cycle losses [15]. Ge et al. have created an exergy-based model for the ecological performance of the air standard irreversible Otto cycle [16].

It is possible to find many studies in the literature besides these. Air-standard or air-fuel assumtion can be done with FTT models [17, 18]. However, it is possible that the specific heats do not change with temperature [11,19], or that the specific heat changes linearly, logarithmically, exponentially or polynomally [20-22]. Numerical examples are also included in the studies. In air-fuel assumtion models, it is also possible to examine concepts related to combustion such as residual gas fraction, equivalence ratio and combustion efficiency. In addition, ecological performance analysis can be done using the second law concepts. For heat transfer and friction losses, various models in the literature can be used [5-27].

In this study, FTT model was constructed to investigate the effect of residual gas fraction and mean piston speed on the cycle performance by using constant specific heat in consideration of heat transfer, friction and irreversibilities in Otto cycle of air-fuel assumption and these effects were investigated with a numerical example. In addition, residual gas temperature is included in the calculation for the initial cycle temperature.

2. METHODS

The pressure-volume (*P-v*) and the temperature-entropy (*T-s*) diagrams of an irreversible four-stroke Otto engine cycle is shown in Fig. 1, where the "*s*" subscripts denote reversible processes for compression (1→2*s*) and expansion (3→4*s*). 1→2 and 3→4 are processes in which internal irreversibilities are accounted for. The heat addition (2→3) and the heat rejection (4→1) processes are isochoric processes [23].

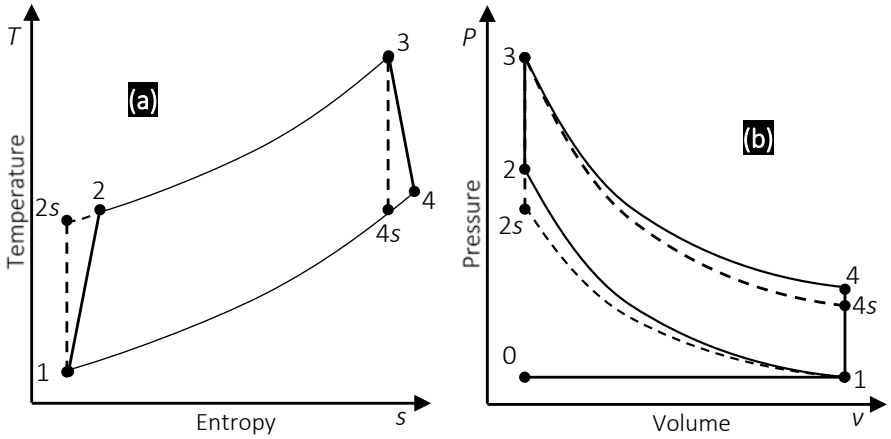

Fig. 1. *Otto cycle (a) Ts diagram, (b) Pv diagram*

The relations between the fuel flow ($\dot{m}_f$) and mean piston speed (S_p) [8], between $\dot{m}_f$ and the fuel-air-residual gas (mixture) flow ($\dot{m}_t$) [23] are defined as:

$$\dot{m}_f = 0.0003\bar{S}_p \quad (1)$$

$$\dot{m}_t = \dot{m}_f + \dot{m}_a + \dot{m}_r = \frac{\dot{m}_f(\phi + x_{AFs})}{\phi(1 - x_r)} \quad (2)$$

where $x_{AFs}, \dot{m}_a$, ϕ and x_r, are the air-fuel ratio for stoichiometric conditions, air flow, equivalance ratio and the residual gas fraction from previous cycle, respectively. Residual gas fraction can find it as [23]:

$$x_r = \frac{\dot{m}_r}{\dot{m}_t} \quad (3)$$

where $\dot{m}_r$ is residual gases flow. It should be noted here that the residual gases were assumed to consist of CO_2, H_2O and N_2.

The specific heat at constant volume (c_{vt}) and the gas constant (R_t) for the working fluid are defined as:

$$c_{vt} = \frac{\left\{\begin{matrix}(1 - x_r)\left(x_{AFs}c_{va} + \phi c_{vf}\right) \\ +x_r(\phi + x_{AFs})c_{vr}\end{matrix}\right\}}{(\phi + x_{AFs})} \quad (4)$$

$$R_t = \frac{\left\{\begin{matrix}(1 - x_r)\left(x_{AFs}R_a + \phi R_f\right) \\ +x_r(\phi + x_{AFs})R_r\end{matrix}\right\}}{(\phi + x_{AFs})} \quad (5)$$

where c_{va}, c_{vf} and c_{vr} are the mass specific heat at constant volume for air, fuel and residual gases, and R_a R_f,and R_r are the gas constant for air, fuel and residual gases, respectively.

For the two adiabatic processes, the compression and expansion efficiencies [24]:

$$\eta_c = (T_{2s} - T_1)/(T_2 - T_1) \quad (6)$$

$$\eta_e = (T_4 - T_3)/(T_{4s} - T_3) \quad (7)$$

These two efficiencies are used to describe the internal irreversibility of the processes. The equations for reversible adiabatic processes 1→2s and 3→4s are as follows [21]:

$$c_{vt}\ln(T_{2s}/T_1) = R_t\ln(\varepsilon) \quad (8)$$

$$c_{vt}\ln(T_{4s}/T_3) = -R_t\ln(\varepsilon) \quad (9)$$

The added heat flow per second in the isochoric (2→3) heat addition process may be written as [26]:

$$\dot{Q}_{in} = \dot{m}_t c_{vt}(T_3 - T_2) \quad (10)$$

The rejected heat flow per second in the isochoric (4→1) heat rejection process may be written as [22]:

$$\dot{Q}_{out} = \dot{m}_t c_{vt}(T_4 - T_1) \quad (11)$$

The total energy flow of the fuel may be written as [23]:

$$\dot{Q}_f = \eta_{com}\dot{m}_f H_u \quad (12)$$

where η_{com} is the combustion efficiency and can be accepted as 0.87 [9]. H_u is the lower heat value of the fuel.

Heat transfer losses for an ideal Otto cycle model can be negligible, but for a real Otto cycle, the heat transfer irreversibility between the working fluid and the cylinder wall is so important that it can not be negligible. The heat loss on the cylinder wall can be expressed by a simple linear equation.

$$\dot{Q}_{ht} = \dot{m}_t\beta(1 - x_r)(T_2 + T_3 - 2T_w) \quad (13)$$

where β is the heat loss coefficient of the cylinder wall.

The relatioship between $\dot{Q}_f$, $\dot{Q}_{in}$ and$\dot{Q}_{ht}$ can be defined as follows [24]:

$$\dot{Q}_{in} = \dot{Q}_f - \dot{Q}_{ht} \quad (14)$$

In thermodynamic analyzes T_1 is considered a constant value as the initial cycle temperature. The T_1 is defined as a specific function because the residual gas fraction is now included in the calculation. It is assumed that T_1 changes according to reference temperature (T_0), T_4 and x_r. T_1 may be written as:

$$T_1 = T_0 + \frac{x_r R_r(T_4 - T_0)}{R_t} \quad (15)$$

The friction loss can be expressed as a function of S_p [24]:

$$P_\mu = -\mu\left(S_p\right)^2 \quad (16)$$

where μ is the coefficient of friction, which takes into account the global losses.

The effective power output (P_e) of the Otto cycle engine is expressed by:

$$P_e = \dot{Q}_{in} - \dot{Q}_{out} - \left|P_\mu\right| \quad (17)$$

In this study, fuel consumption is expressed as a function of meanpiston speed. For this reason, the amount of energy input depends on the mean piston speed. To make a fair comparison, the power output is dimensionless according to the initial conditions. The dimensionless power output (ψ) is expressed as follows:

$$\psi = \frac{P_e}{\dot{m}_t R_t T_1} \quad (18)$$

The efficiency of the cycle is expressed by [24]:

$$\eta_{th} = P_e/\dot{Q}_f \quad (19)$$

When S_p, c_{va}, c_{vf}, c_{vr}, R_a, R_f, R_r, β, T_w, T_0, μ, x_r, x_{AFs} and ϕ are given, temperatures of the critical points (T_1, T_2, T_{2s}, T_3, T_4, and T_{4s}) can be obtained from Eqs. (7-16). Using Eqs. (17-19), power output, dimensionless power output and thermal efficiency can be determined, respectively.

3. RESULTS AND DISCUSSION

The following constants and parameters are used for the numerical example (Table 1):

Table 1. *Parameters used for numerical example* [5-27]

Parameter	Value	Parameter	Value
η_c	0.97	η_e	0.97
x_{AFs}	15.05	T_0	300 K
β	0.5 kJ/kgK	T_w	400 K
μ	12.9 Ns/m	H_u	44790 kJ/kg
c_{va}	0.718 kJ/kgK	R_a	0.287 kJ/kgK
c_{vf}	1.638 kJ/kgK	R_f	0.073 kJ/kgK
c_{vr}	0.866 kJ/kgK	R_r	0.307 kJ/kg
ϕ	1.00	x_r	5%→15%
ε	2→100	S_p	7→15 m/s

This study focuses on the investigation of the effects of mean piston speed and residual gas fraction on performance of a four-stroke irreversible Otto cycle engine. The performance parameters obtained for both engines are compared.

The variation of critical point temperatures with respect to thermal efficiency is given in Fig 2. In addition, the dashed line shows the relationship between thermal efficiency and compression ratio.

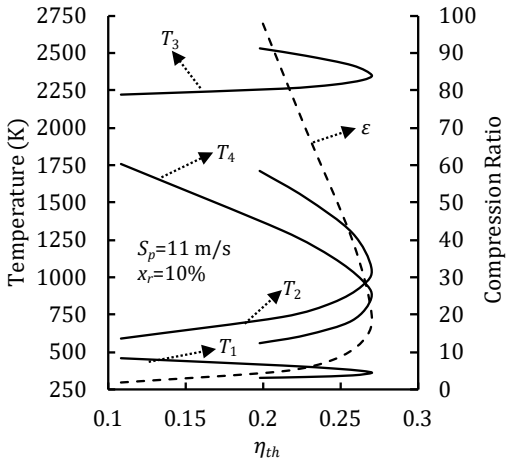

Fig. 2. *The temperature versus thermal efficiency*

In Fig. 2, the thermal efficiency increases to a certain compression ratio and the thermal efficiency begins to decrease at higher compression ratios. It is seen that T_1 decreased with the increase of η_{th}. In the case where the η_{th} is maximum, T_1 is almost minimum. T_2 is the optimum value at the point where the η_{th} is maximum. Increasing T_2 after this value increases the compression ratio. When T_3 is examined, it has a similar characteristic depending on T_2. The continuation of increase of T_3 after the maximum η_{th} is due to the increase of the compression ratio as in T_2. The same is true for the T_4.

Figs. (3-6) show the effect of the mean piston speed on the cycle performance. Figs. (7-10) show the effect of the residual gas fraction on the cycle performance.

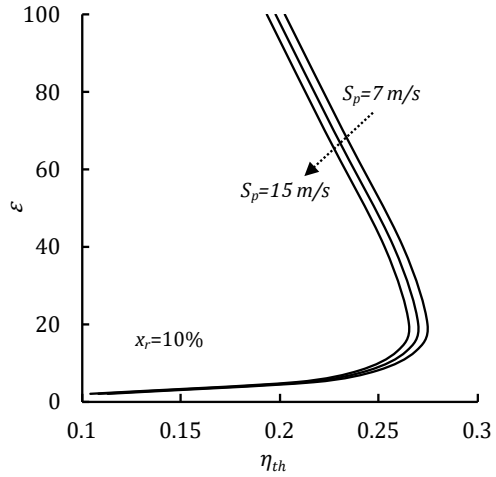

Fig. 3. *Effect of mean piston speed on the variation of the compression ratio with thermal efficiency*

Fig. 3 shows the change in compression ratio due to thermal efficiency. As the mean piston speed increases, the maximum thermal efficiency decreases. While the thermal efficiency increases to a certain compression ratio, lower thermal efficiency is obtained at higher compression ratios. However, as the mean piston speed increases, the same thermal efficiency can be achieved at lower compression ratios. Although higher maximum thermal efficiency can be achieved at low mean piston speed, it is more advantageous that the mean piston speed is high at the compression ratios after the maximum thermal efficiency.

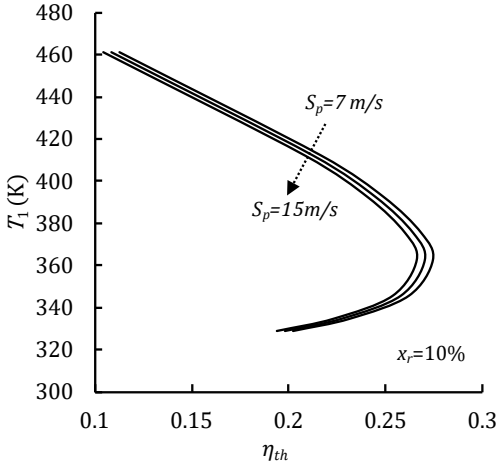

Fig. 4. *Effect of mean piston speed on the variation of the initial temperature with thermal efficiency*

Fig. 4 shows the change in the initial temperature T_1 with respect to the thermal efficiency. As the mean piston speed increases T_1 decreases. In addition, the higher mean piston speed, the higher thermal efficiency is achieved. The increase in T_1 after reaching maximum thermal efficiency is due to the increased compression ratio.

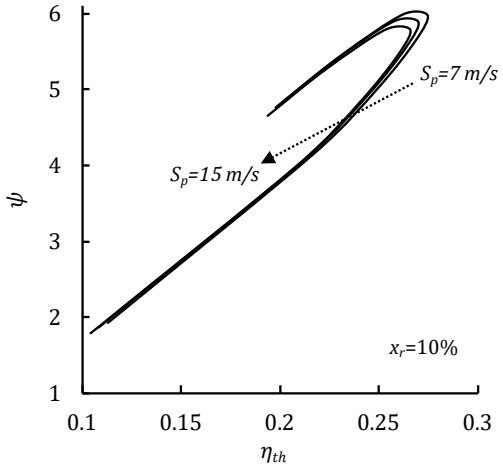

Fig. 5. *Effect of mean piston speed on the variation of the dimensionless power output with thermal efficiency*

Fig. 5 shows the variation of the dimensionless power output with respect to the thermal efficiency. As the mean piston speed increases, less thermal efficiency is obtained and less dimensionless power output is obtained. Approximate maximum dimensionless power output is obtained at the point where maximum thermal efficiency is obtained. In fact, the maximum dimensionless power output is obtained at a compression ratio slightly higher than the compression ratio at which the maximum thermal efficiency is obtained.

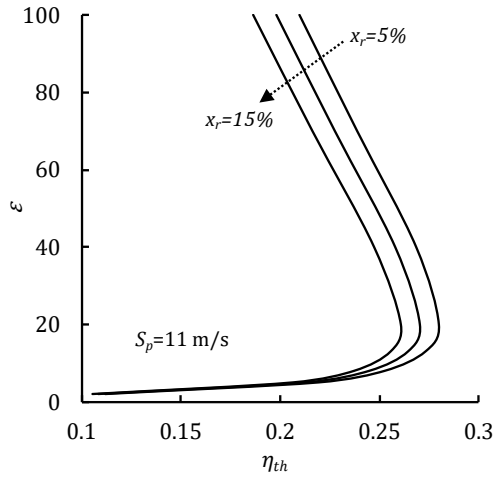

Fig. 6. *Effect of residual gas fraction on the variation of the compression ratio with thermal efficiency*

Figure 6 shows the change in the compression ratio with respect to the thermal efficiency. As the residual gas fraction increases, the maximum thermal efficiency decreases.

Fig. 7 shows the change in T_1 depending on the thermal efficiency. As the residual gas fraction increases, the maximum thermal efficiency decreases and T_1 increases. The reason for the increase in T_1 with the increase of the residual gas fraction is that the temperature of the residual gases is higher than the fresh mixture temperature. In many models in the literature, T_1 is considered as a constant value. In this study, T_1 is modeled as a function of T_4 and residual gas fraction.

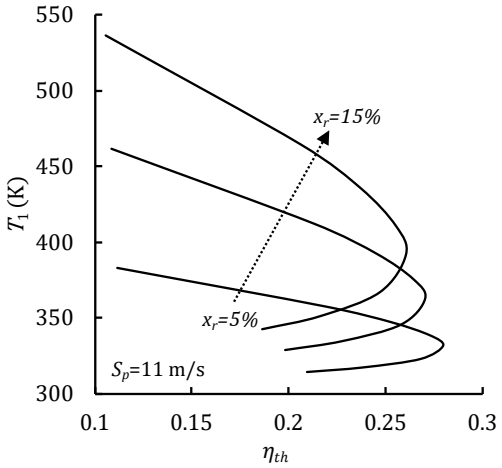

Fig. 7. *Effect of residual gas fraction on the variation of the initial temperature with thermal efficiency*

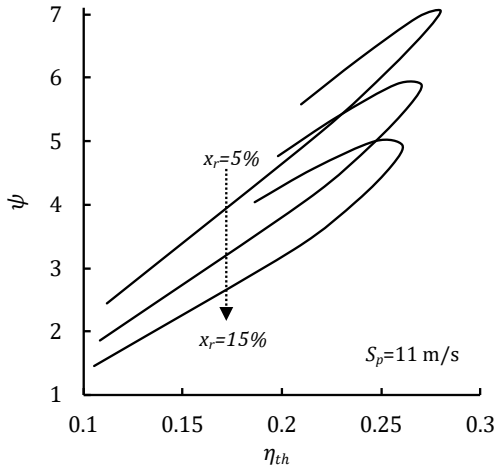

Fig. 8. *Effect of residual gas fraction on the variation of the dimensionless power output with thermal efficiency*

Fig. 8 shows the change in dimensionless power output as a function of heat transfer. The residual gas fraction is significantly reduced and the dimensionless power output is reduced. Therefore, the dimensionless power output is higher in the low residual gas quantity.

4. CONCLUSION

In this study, four-stroke irreversible Otto cycle are modeled using the finite time thermodynamics (FTT). The effects of the mean piston speed and residual gas fraction on the engine performance of the FTT model are

investigated with a numerical example and the results are discussed. In the literature, there has been no study of the effect of residual gas fraction and mean piston speed on the irreversible Otto cycle. However, a function has been derived for the initial temperature using the end-of-cycle temperature and the residual gas fraction.. As a result of this study, the following general results were obtained:

- The thermal efficiency increases up to a certain compression ratio and the thermal efficiency decreases after this compression ratio.
- If the thermal efficiency is maximum, the initial cycle temperature is optimum. Then the initial cycle temperature is also increased by the effect of the compression ratio.
- As the mean piston speed increases, the maximum thermal efficiency that can be obtained from the cycle decreases.
- As the residual gas fraction increases, the initial cycle temperature increases.
- As the residual gas fraction increases, the maximum thermal efficiency that can be obtained from the cycle decreases.
- Dimensionless power output is higher at low piston speed and low residual gas fraction.

With this study, the results that engine designers can benefit from have been obtained. In addition, since the model of the FTT model is used instead of the classical thermodynamic model, the theoretical cycle is further approximated to the actual cycle, and the effect of the engine performance on the independent parameters such as mean piston speed and residual gas fraction can be examined.

NOMENCLATURES

c_{va}	[kJ/kgK]	Specific heat for air
c_{vf}	[kJ/kgK]	Specific heat for fuel
c_{vr}	[kJ/kgK]	Specific heat for residual gas
c_{vt}	[kJ/kgK]	Specific heat for mixture
H_u	[kJ/kg]	Lower heat value for fuel
$\dot{m}_a$	[kg/s]	Air flow
$\dot{m}_f$	[kg/s]	Fuel flow
$\dot{m}_r$	[kg/s]	Residual gas flow
$\dot{m}_t$	[kg/s]	Mixture flow
P_e	[kW]	Effective Power output
P_μ	[kW]	Global friction loss power
$\dot{Q}_{ht}$	[kJ/s]	Heat leakage per second
$\dot{Q}_f$	[kJ/s]	Fuel energy flow
$\dot{Q}_{in}$	[kJ/s]	Added heat flow
$\dot{Q}_{out}$	[kJ/s]	Rejected heat flow
R_a	[kJ/kgK]	Gas constant for air
R_f	[kJ/kgK]	Gas constant for fuel
R_r	[kJ/kgK]	Gas constant for residual gas
R_t	[kJ/kgK]	Gas constant for mixture
S_p	[m/s]	Mean piston velocity
T_0	[kJ/kgK]	Reference temperature
T_w	[kJ/kgK]	Wall temperature
x_{AFs}	[-]	Stoichiometric air-fuel ratio
x_r	[-]	Residual gas fraction
η_c	[-]	Compression efficiency
η_{com}	[-]	Combustion efficiency
η_e	[-]	Expansion efficiency
η_{th}	[-]	Thermal efficiency
Φ	[-]	Equivalence ratio
β	[kJ/kgK]	Heat leakage coefficient
ε	[-]	Compression ratio
μ	[Ns/m]	Coefficient of friction
ψ	[-]	Dimensionless power output

REFERENCES

[1]. Ge, Y., Chen, L., & Qin, X. (2018). Effect of specific heat variations on irreversible Otto cycle performance. *International Journal of Heat and Mass Transfer*, vol. 122, p. 403-409, DOI: 10.1016/j.ijheatmasstransfer.2018.01.132.

[2]. Xu, J., Zheng, Y., Wang, Y., Yang, X., Yu, C., Xie, X., ... & Zhao, X. (2017). An actual thermal efficiency expression for heat engines: effect of heat transfer roadmaps. *International Journal of Heat and Mass Transfer*, vol. 113, p. 556-568, DOI: 10.1016/j.ijheatmasstransfer.2017.05.104.

[3]. Bejan, A. (2013). *Entropy generation minimization: the method of thermodynamic optimization of finite-size systems and finite-time processes*. CRC press.

[4]. Caton, J. A. (2002). Illustration of the use of an instructional version of a thermodynamic cycle simulation for a commercial automotive spark-ignition engine. *International Journal of Mechanical Engineering Education*, vol. 30, p. 283-297, DOI: 10.7227/IJMEE.30.4.1.

[5]. Wu, Z., Chen, L., Ge, Y., & Sun, F. (2017). Power, efficiency, ecological function and ecological coefficient of performance of an irreversible Dual-Miller cycle (DMC) with nonlinear variable specific heat ratio of working fluid. *The European Physical Journal Plus*, vol.132(5), p.(203)1-17 DOI: 10.1140/epjp/i2017-11465-1.

[6]. Berry, R. S. (2000). *Thermodynamic optimization of finite-time processes*. J. Wiley.

[7]. Chen, L. (2004). *Advances in finite time thermodynamics: analysis and optimization*. Nova Publishers.

[8]. Chen, L. G., & Xia, S. J. (2016). Generalized thermodynamic dynamic-optimization for irreversible processes.

[9]. Ge, Y., Chen, L., Qin, X., & Xie, Z. (2017). Exergy-based ecological performance of an irreversible Otto cycle with temperature-linear-relation variable specific heat of working fluid. *The European Physical Journal Plus*, vol. *132*(5), p. (209)1-10, DOI: 10.1140/epjp/i2017-11485-9.

[10]. Ge, Y., Chen, L., & Sun, F. (2016). Progress in finite time thermodynamic studies for internal combustion engine cycles. *Entropy*, vol.18(4), p.139 DOI: 10.3390/e18040139

[11]. Wu, Z., Chen, L., & Feng, H. (2018). Thermodynamic optimization for an endoreversible Dual-Miller cycle (DMC) with finite speed of piston. *Entropy*, vol. *20*(3), p. 165, DOI: doi.org/10.3390/e20030165.

[12]. Ebrahimi, R. (2010). Effects of Variable Specific Heat Ratio on Performance of an Endoreversible Otto Cycle. *Acta Physica Polonica, A.*, vol.117(6) p. 887-891, DOI: 10.12693/APhysPolA.117.887.

[13]. Chen, L., Wu, C., Sun, F., & Cao, S. (1998). Heat transfer effects on the net work output and efficiency characteristics for an air-standard Otto cycle. *Energy conversion and management*, vol.

39(7), p. 643-648, DOI: doi.org/10.1016/S0196-8904(97)10003-6.

[14]. Hou, S. S. (2007). Comparison of performances of air standard Atkinson and Otto cycles with heat transfer considerations. *Energy Conversion and Management*, vol. 48(5), p. 1683-1690, DOI: 10.1016/j.enconman.2006.11.001.

[15]. Ge, Y., Chen, L., Qin, X., & Xie, Z. (2017). Exergy-based ecological performance of an irreversible Otto cycle with temperature-linear-relation variable specific heat of working fluid. *The European Physical Journal Plus*, vol. *132*(5), p. (209)2-9, DOI: 10.1140/epjp/i2017-11485-9.

[16]. Ge, Y., Chen, L., & Sun, F. (2013). Ecological optimization of an irreversible Otto cycle. *Arabian Journal for Science and Engineering*, vol. 38(2), p. 373-381, DOI: . 10.1007/s13369-012-0434-8.

[17]. Ebrahimi, R., & Hoseinpour, M. (2013). Performance analysis of irreversible Miller cycle under variable compression ratio. *Journal of Thermophysics and Heat Transfer*, vol. 27(3), p. 542-548, DOI: 10.2514/1.T3981

[18]. Sieniutycz, S., & Shiner, J. S. (1994). Thermodynamics of irreversible processes and its relation to chemical engineering: Second law analyses and finite time thermodynamics. *Journal of Non-Equilibrium Thermodynamics*, *19*(4), 303-348, DOI: 10.1515/jnet.1994.19.4.303.

[19]. You, J., Chen, L., Wu, Z., & Sun, F. (2018). Thermodynamic performance of Dual-Miller cycle (DMC) with polytropic processes based on power output, thermal efficiency and ecological function. *Science China Technological Sciences*, vol. *61*(3), p. 453-463, DOI: 10.1007/s11431-017-9108-2.

[20]. Wu, Z., Chen, L., Ge, Y., & Sun, F. (2018). Thermodynamic optimization for an air-standard irreversible Dual-Miller cycle with linearly variable specific heat ratio of working fluid. *International Journal of Heat and Mass Transfer*, vol. 124, p. 46-57, DOI: 10.1016/j.ijheatmasstransfer.2018.03.049.

[21]. Mousapour, A., Hajipour, A., Rashidi, M. M., & Freidoonimehr, N. (2016). Performance evaluation of an irreversible Miller cycle comparing FTT (finite-time thermodynamics) analysis and ANN (artificial neural network) prediction. *Energy*, vol. 94, p. 100-109, DOI: 10.1016/j.energy.2015.10.073.

[22]. Gonca, G., & Sahin, B. (2017). Effect of turbo charging and steam injection methods on the performance of a Miller cycle diesel engine (MCDE). *Applied Thermal Engineering*, vol.118, p. 138-146, DOI: 10.1016/j.applthermaleng.2017.02.039.

[23]. Ebrahimi, R. (2013). Thermodynamic Modeling of an Atkinson Cycle with respect to Relative Air-Fuel Ratio, Fuel Mass Flow Rate and Residual Gases. *Acta Physica Polonica, A*., vol. 124, no. 1 p. 29-34, DOI:10.12693/APhysPolA.124.29.

[24]. Ebrahimi, R. (2011). Effects of mean piston speed, equivalence ratio and cylinder wall temperature on performance of an Atkinson engine. *Mathematical and Computer Modelling*, vol. 53, no. 5-6, p. 1289-1297, DOI:10.1016/j.mcm.2010.12.015.

[25]. Ebrahimi, R. (2018). Effect of Volume Ratio of Heat Rejection Process on Performance of an Atkinson Cycle. *Acta Physica Polonica A*, vol. 133, no. 1, p. 201-205, DOI:10.12693/APhysPolA.133.201.

[26]. Ge, Y., Chen, L., Sun, F., & Wu, C. (2005). Thermodynamic simulation of performance of an Otto cycle with heat transfer and variable specific heats of working fluid. *International Journal of Thermal Sciences*, vol. 44 no. 5, p. 506-511, DOI:10.1016/j.ijthermalsci.2004.10.001.

[27]. Zhao, Y., & Chen, J. (2007). An irreversible heat engine model including three typical thermodynamic cycles and their optimum performance analysis. *International Journal of Thermal Sciences*, vol. 46, no. 6, p. 605-613, DOI:10.1016/j.ijthermalsci.2006.04.005.

Techno-Science

Scientific Journal of Mehmet Akif Ersoy University

www.dergipark.gov.tr/sjmakeu

WEB BASED TRACKING OF VEHICLE FAULT AND PERFORMANCE DATA ON OBD II

Ahmet Ali SÜZEN[1*], Kıyas KAYAALP[1]

[1] *Department of Computer Technologies, Applied Sciences University of Isparta, Turkey*

ARTICLE INFO

Article History

Received : 24/09/2018
Revised : 30/09/2018
Accepted : 30/09/2018
Available online : 30/09/2018

Keywords

Arduino
OBD II
Vehicle tracking
Web Based

ABSTRACT

OBD (On-board Diagnostic) is the standard used by the SAE (Society of Automotive Engineers) in 1988 to monitor the data flow of sensors from external sources. OBD was updated as OBD II standard in 1990. Nowadays, monitoring of the flow of sensor data in vehicles is done via OBD-II standard. The OBD-II connection, which must be used in all vehicles, is a window that opens out of a vehicle.In this study, the data received via OBD II via Bluetooth was transferred to the Web via Arduino Uno development card. The error codes and speed-fuel information produced by the vehicle during the journey were transferred to the software in the Web environment with the arduino with wifi module. The software developed with ASP.NET converts incoming error codes into meaningful texts. This allows the first intervention to be carried out by the experts in the event of a failure during the driving. The internet required for the operation of the system is provided by sharing the personal access point of the driver's mobile device internet (hotspot).

1. INTRODUCTION

Electronic control units (ECU) used in vehicles are also the black box of the vehicles. Parameters for vehicle safe use and the parameters to be used in undesired situations during vehicle use are stored on the ECU. For a vehicle equipped with an ECU, situations such as the occurrence of an error, temporary or permanent condition, or the components that affect it, whether it affects the use of the vehicle are important and such information is continuously recorded and the driver is informed on the trip computer screen in the vehicle [1].

The ECU also controls precise control of the engine's main features, such as ignition timing, fuel injection functions, variable valve timing, idle speed, as well as other vehicle systems such as the transmission, brake and steering systems. ECU's total control of these systems never means that the system will work perfectly. Both external factors and internal factors can cause temporary or permanent problems in vehicles. Some of these problems may not interfere with the operation of the vehicle. However, as soon as possible to diagnose a possible fault is vital for both driving safety and vehicle safety [2].

It is always important that the faults that occur in the vehicles are given in a simple way. It is a basic principle to give general information instead of instantaneous details for the drivers, but only for signs of faults. The details of the fault are important only for the expert repairman. However, some faults may not be directly related to the part of the fault. This situation can be compared to human diseases. The symptom of a disease can be seen as a condition of an organ that is not directly related to the disease. The situation is the same for faults occurring in vehicles. It is not necessary for the driver to be informed in detail by the vehicle in such cases as an expert is required for this to be understood [1-2].

The output required for the transfer of this error information stored in the ECU is OBD, which is an abbreviation for “On-Board Diagnostic” words [1]. The output required for the transfer of this error information stored in the ECU is OBD, which is an abbreviation for on-board diagnostical words. Although the history dates back to 1988, especially in all vehicles produced in 2000 and later, there are OBD connectors. The OBD connector is the external door of the ECU, a black box of a vehicle. The OBD connector used today is called the OBD-II or OBD-2. The OBD-I connector is not standardized between

* Corresponding Author: ahmetsuzen@isparta.edu.tr

To cite this article: Suzen, A., Kayaalp, K. (2018). Web based tracking of vehicle fault and performance data on OBD II. *Techno-Science* vol. 1, no. 1 p. 13-16.

firms, and therefore the OBD-II connector, which is a standard (universal) connector in 1996, has started to be used [3].

Communication with OBD-II can be wired or wireless. OBD-II adapters are used for this purpose. In this study, a commercially available OBD-II adapter with bluetooth communication is used. The main purpose of this study is to create a Web based fault tracking system by means of data collection device which we designed by using Arduino development card, bluetooth module and wifi module.

2. METHODS

2.1. Service-PID codes for OBD-II

The SAE J1962 is an accepted standard for the OBD-II connector and communication. For OBD-II, two connection types A and B type have been determined. The type A connector is used for 12V and the type B connector for vehicles using 24V supply voltage. Two connector types are shown in Figure 1. Both consist of 16-pin (2x8) D-shaped connectors [4].

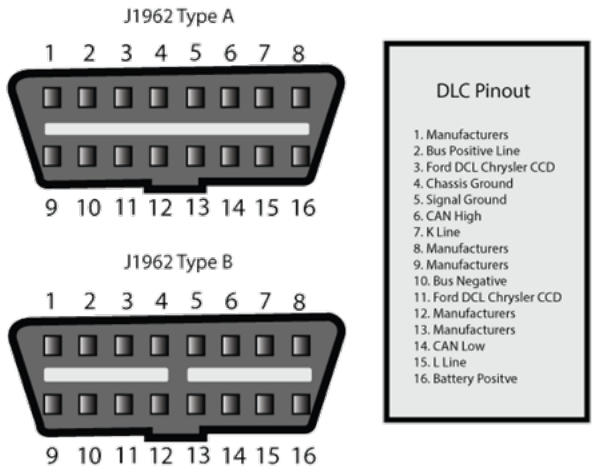

Fig. 1. *OBD-II connector wiring* [5]

As shown in Figure 1, the OBD-II connector has battery (power supply), communication and manufacturer pins. The manufacturer pins are special pins that allow certain special data to be received and that the ECU can be partially programmed, which changes according to each manufacturer and acts as a second key.

No significant direct data can be obtained through the ECU. For this purpose, a special parameter identification (OBD-PID) has been created for OBD. The SAE J1979 standard for OBD-PID has been adopted [6].

A total of 10 service parameters were determined in 2017 for OBD-PID. These service parameters are hex codes that can be requested from the ECU, such as displaying the available data, displaying the registered diagnostic error codes, clearing diagnostic error codes and stored values, displaying the test results, testing vehicle components, displaying vehicle information, displaying permanent diagnostic error codes. Service parameters may vary depending on the manufacturer. PID hex code is generated after service hex code (Table 1). The service and PID hex code correspond to the requested response from the ECU again as the hex code. Further information can be found in Ref [6].

Table 1. *Service-PID hex code examples* [6]

Service-PID hex code	Description	Formula
01-04	Calculated engine load (%)	$\frac{100}{255}A$
01-0C	Engine rpm (rpm)	$\frac{256A+B}{4}$
01-0E	Timing advance (° BTDC)	$\frac{A}{2}-64$
01-5E	Engine fuel rate (L/h)	$\frac{256A+B}{20}$

The 4-byte A, B, C, and D hex values come from the ECU according to the Service-PID hex code. The values of A and B in Table 1 refer to desimal numbers. The obtained values of A and B are converted to decimal numbers to obtain the desired information. C and D values are used in other service-PID hex codes.

2.2. Bluetooth adapter for OBD-II

The most common OBD-II adapter on the market is bluetooth communication. These adapters are called ELM-327, which is the code used for the integration. MCP-2551 is used for communication of ELM-327 with CAN. The communication with the ECU can be achieved with these two integrated tools. Wired or wireless communication can be used to transmit this communication to an external device. The adapter used in this study is ELM 327 integrated and has bluetooth communication [7].

Fig. 2. *Bluetooth OBD-II adapter* [8]

It is possible to find many software used with OBD-II adapter. These softwares generally show specific instant data. Manufacturer's software is designed to perform all operations on ECU. Figure 3 shows various software interfaces.

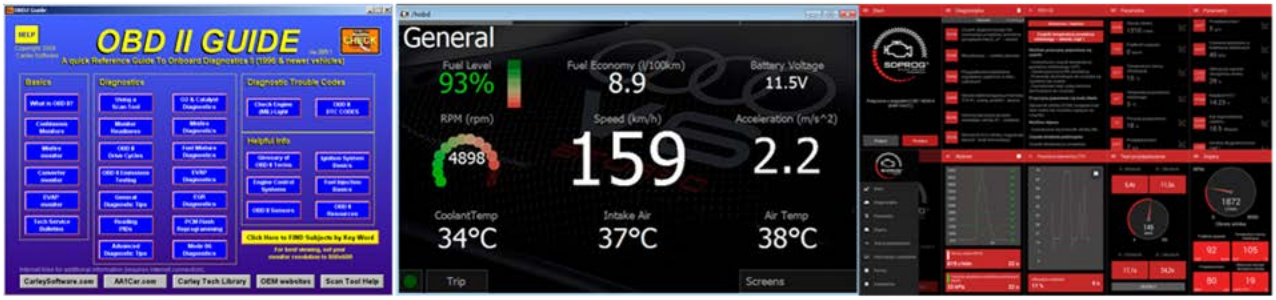

Fig. 3. *OBD-II softwares* [9-11]

In this study, a simple controller and software which can communicate with the OBD-II adapter via bluetooth and transfer the data obtained via wifi to the remote device has been created.

2.3. OBD-II Control Device

In this study, vehicle data were requested at 1 minute intervals via Arduino. The data was transferred to Arduino with the OBD-II Bluetooth adapter pluged into the vehicle. The data were processed with arduino and recorded in the database on the Web. Thanks to the Web interface, data recorded in the database can be analyzed. The HC-05 bluetooth module is used for communication with the OBD-II bluetooth adapter and the ESP-8266 wifi module is used for data transfer to the Web (Figure 4).

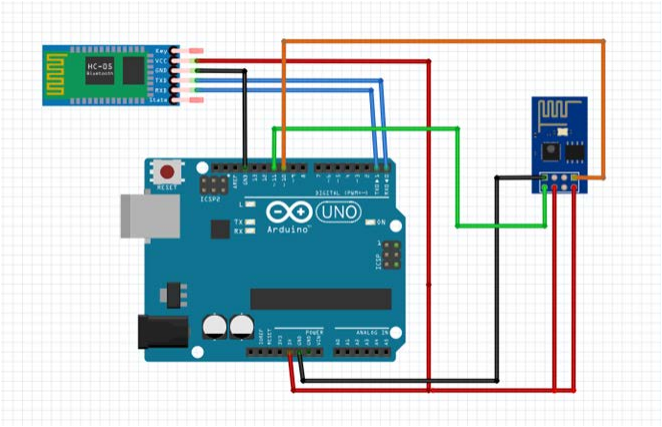

Fig. 4. *OBD-II control device*

For the Arduino software to work, the Initialization operation must be performed first. ELM327 works with AT (Attention) commands. Therefore, it is necessary to perform the Initialization process with AT commands and make the device ready. On the Arduino IDE, this process was performed with the following code block (Figure 5)

After the service-PID hex code sent to the ECU, the ECU receives a response. For example, when the hex code 01-5E is sent, a hex-code, aa-bb-cc-dd, is returned. The values here can be converted to decimals to obtain the required values A, B, C and D for the formula. In order to obtain the registered error codes on the vehicle, serial port listening is performed. A 5 digit error code (XXX XX) comes from this listening. The error definitions corresponding to this error code are listed in the Diagnostic Trouble Code (DTC) list as standard and total 3170 for year 2017. Error codes can also be defined by matching them on the Web. A DTC code is encoded as shown in figure 6.

```
SoftwareSerial elm327(0, 1);
      elm327.begin(9600);
      elm327. println ("ATZ");
            delay(2000);
      elm327. println ("ATEO");
            delay(1000);
      elm327. println ("ATL0");
            delay(500);
      elm327. println("ATH1");
            delay(500);
      elm327. println ("ATSP 5")
            delay(500);
      elm327. println ("01 00");
            delay(500);
```

Fig. 5. *AT code block*

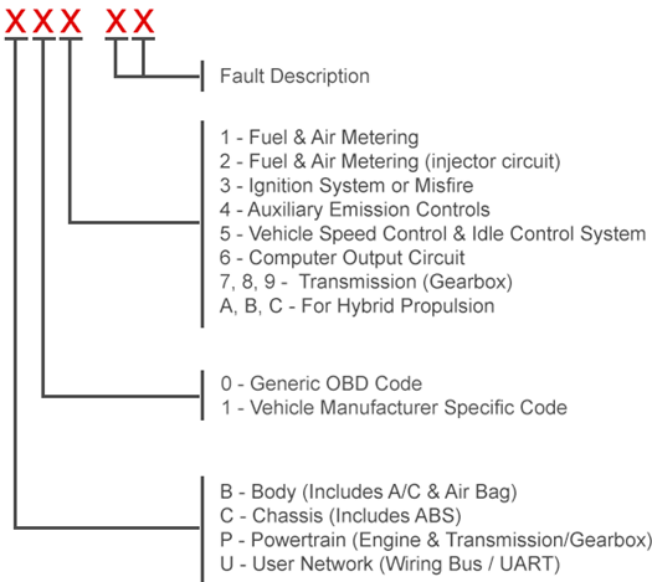

Fig. 6. *Explanation of the DTC codes* [12]

3. RESULTS AND DISCUSSION

It is provided to monitor the data coming from the vehicle in the Web interface of the actual study. The web interface is developed using C# programming language with ASP.NET. The vehicle data received with the Arduino development card is displayed as a querystring

parameter as shown in on the web page with the wifi module:

http://localhost:60904/DataSave.aspx?Gas=10&EngineTemp=40&Power=2000&Speed=0&DTC=P0157

These parameters are taken from the browser address section and saved in the database. Technical data can be accessed via the interface via the interface shown in Figure 7.

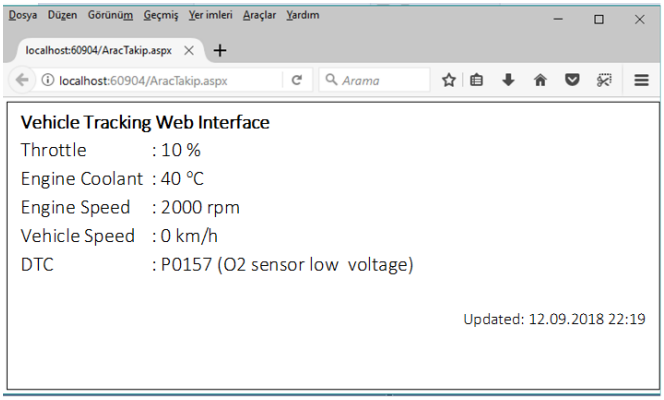

Fig. 7. *Vehicle tracking Web interface*

4. CONCLUSIONS

The work carried out via OBD-II bluetooth device allows the monitoring of data about the vehicle on the Web with the help of Arduino. With this vehicle tracking software, it is possible to control the DTC error codes, speed, temperature and power stored in the vehicle in web environment. The system provides quick and accurate measures to prevent possible problems during driving or when the technical expert is away. It is aimed to provide emergency measures against the error codes during vehicle driving with expert support. In addition to this, it is planned to carry out a process such as making a transaction that the driver can do about the error codes obtained by using artificial intelligence algorithms in future studies. Today, when autonomous vehicles are developed, such applications are expected to become a necessity in the near future.

ACKNOWLEDGEMENTS

This paper was developed and derived from the paper presented by the authors at the 1st International Vocational Science Symposium.

REFERENCES

[1]. Baek, S. H., & Jang, J. W. (2015). Implementation of integrated OBD-II connector with external network. *Information Systems*, *50*, 69-75, DOI: 10.1016/j.is.2014.06.011.

[2]. Yang, L., Zhang, S., Wu, Y., Chen, Q., Niu, T., Huang, X., ... & Hao, J. (2016). Evaluating real-world CO2 and NOX emissions for public transit buses using a remote wireless on-board diagnostic (OBD) approach. *Environmental pollution*, *218*, 453-462, DOI: 10.1016/j.envpol.2016.07.025

[3]. OBD Advisor, *https://www.obdadvisor.com/difference-obd1-obd2-scanners/,* accessed on 2018-09-20.

[4]. SAE J1962, *https://www.sae.org/standards/content/j1962_201207/,* accessed on 2018-09-20.

[5]. Obd Connector Wiring, *http://osomeweb.com/obd-connector-wiring.html*, accessed on 2018-09-20.

[6]. SAE J1979, *https://www.sae.org/standards/content/j1979_201202/,* accessed on 2018-09-20.

[7]. ELM 327, *https://www.elmelectronics.com/wp-content/uploads/2016/07/ELM327DS.pdf,* accessed on 2018-09-20.

[8]. OBD-II, *https://tr.pinterest.com/pin/387802217909976705/*, accessed on 2018-09-20.

[9]. OBD Software-1, *https://scantoolcenter.com/blog/the-unique-obd-nissan-software/,* accessed on 2018-09-20.

[10]. OBD Software-2, *http://www.archer-soft.com/en/blog/7-best-obd-apps-your-car,* accessed on 2018-09-20.

[11]. OBD Software-3, https://www.elexpress.pl/product-eng-480-Diagnostic-program-SDPROG-OBD2-WIN-iOS-Android-KOD-ID39A.html, accessed on 2018-09-20.

[12]. OBD-II DTC List, *http://www.totalcardiagnostics.com/support/Knowledgebase/Article/View/21/0/complete-list-of-obd-codes-generic-obd2-obdii--manufacturer*, accessed on 2018-09-20.

Techno-Science

Scientific Journal of Mehmet Akif Ersoy University

www.dergipark.gov.tr/sjmakeu

DESIGN, DEVELOPMENT AND CONTROL OF LONG RANGE QUADCOPTER

Syed NAJEEBULLAH[1*], Ajab Khan KASI[1], Jafar Khan KASI[1]

[1] *Department of Physics, University of Balochistan, Quetta, Pakistan*

HIGHLIGHTS

- Designing and developing of all mechanical parts of Quadcopter.
- Developed and designed our own 4G communication module that is compatible to interface with Quadcopter design.
- Replace remote control (RC) communication module with our own made 4G communication module.
- We get freedom to control the Quadcopter from any location of the world where 4G network is available.
- Automatic mission is accomplished with Quadcopter by using GPS base navigation system.

GRAPHICAL ABSTRACT

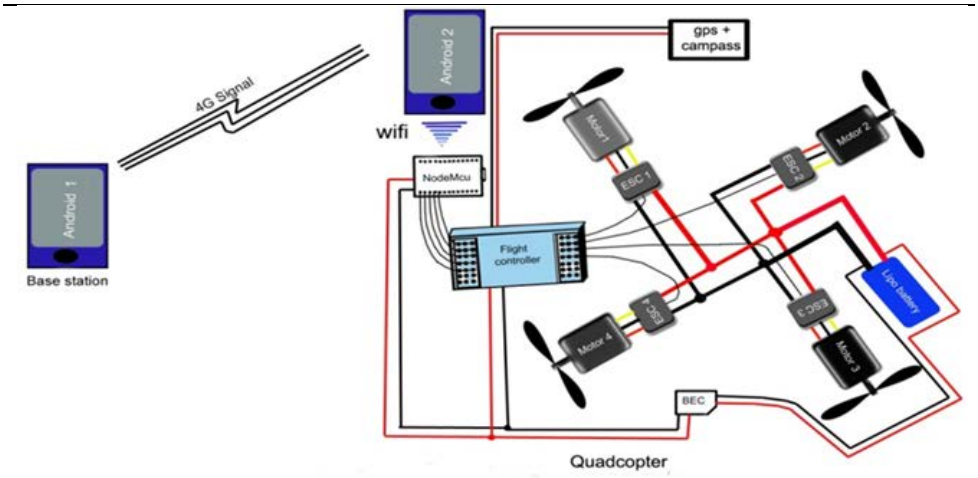

ARTICLE INFO

Article History

Received	:	20/09/2018
Revised	:	26/09/2018
Accepted	:	26/09/2018
Available online	:	30/09/2018

Keywords

Quadcopter
Long Range
4G network
Nodemcu
Mission planner
Automatic mission

ABSTRACT

This research is based on the design, development and control of long range quadcopter using 4G network. The developed Quadcopter has capability to be controlled from any location where 4G network is available. The Quadcopter consist of mainly 4 components including: flight controller, motors and propellers, electronic speed controller and communication module. The first three components are same as used in conventional Quadcopter where as the long range is achieved with the help of unique communication system. The communication module of this Quadcopter consists of Nodemcu with 4G wifi module and android based mobile phone. A graphical user interface is developed in blynk software through which Nodemcu is control which results to control Quadcopter from distant place. 4G based quadcopter has an advantage over conventional RF module based quadcopter which has limited coverage area. Automatic mission is accomplished with Quadcopter using GPS based navigation system.

1. INTRODUCTION

Multi-rotor drone is an unmanned aerial vehicle (UAV), which is to be controlled from the ground station, without pilot on the board using communication module. Multirotor drone has wide range of indoor and outdoor application such as surveillance, aerial photography, agriculture monitoring purposes etc. Multirotor drone is the most prominent drone due to its vertical take-off and landing (VTOL) capability [1-3]. Quadcopter is a type of Multirotor drone consisting of 4 high speed brushless motors, 4 Electronic speed controllers(ESC), 4 propellers, Flight controller, communication module and lipo battery. Quadcopter has two frame configuration, that is '+' and '×' configuration [4]. This paper belongs to '×'configuration of quadcopter frame. Two motors on opposite arms of the

* Corresponding Author: engrr.najeebullahkhan@gmail.com

To cite this article: Najeebullah, S., Kası, A.K., Kası, J.K. (2018). Design, development and control of long range quadcopter. *Techno-Science* vol. 1, no. 1 p. 17-21.

quadcopter frame rotating clockwise (CW) direction, whereas the two motors on the other two opposite arms rotating counter-clockwise (CCW) direction, which compensate the action and reaction effect (Newton's third law), then quadcopter will take-off without producing any torque in the body frame [1-7]. Flight controller is a main controlling board, is a type of MIMO (multiple input, multiple output) system) which takes multiple input control signal from the communication module (i-e thrust, pitch, roll and yaw signals) and perform some necessary action and give control signal to the output of flight controller [8]. The outputs of the flight controller work as a input to the ESC's and the output of ESC's are connected to the four brushless motors. The ESC's takes control signal in the form of PWM from flight controller and then precisely control the speed of the brushless motors. Propeller connected with brushless motors produce thrust in the upward direction depending on the shape and size of the propellers. Communication module is a transceiver that controls the quadcopter from ground station [9]. Dedicated Radio frequency (RF) module has limited coverage area according to their transmitter and receiver range. If such quadcopter is to be used for long distance then these dedicated RF module does not work. This paper introduce unique 4G communication module in the quadcopter, which comprises of Nodemcu having wifi capability and android cell phone connected with the flight controller and another android cell phone with graphical user interface developed in blynk software is on the ground station control the attitude of the quadcopter. Camera of an android cell phone connected with flight controller has been used for live video streaming and dynamics of quadcopter can be seen on another android cell phone on the base station from unlimited range using 4G network and automatic mission has also been accomplished with Quadcopter using GPS based navigation system.

2. QUADCOPTER DYNAMICS

The quadcopter has four arms with "×" configuration frame as shown in Figure 1.

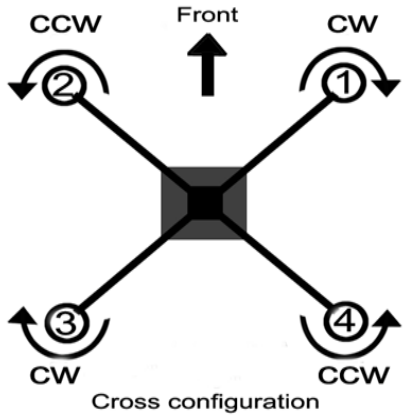

Fig.1. *Show the "×" configuration*

As we explained previously that the quadcopter has four brushless motors on which propellers are mounted, which make the quadcopter has four input forces. Propeller '1' and propeller '3' are moving in clockwise direction, whereas propeller '2' and propeller '4' are moving in counter-clockwise direction. The reason is because when propeller '1' and '3' are moving in clockwise direction, then due to reactive effect the whole body frame of the quadcopter should be moving in counter-clockwise direction (according to Newton's third law) [9-11]. In the same way when propeller '2' and '4' are moving in counter-clockwise direction, then due to reactive effect the whole body frame of the quadcopter should be moving in clockwise direction. If all of the propellers are rotating with the same speed rate, then these two reactive effects will compensate each other and the quadcopter will take-off and landing without producing any torque. If w_1, w_2, w_3 and w_4 represents the rotational speed of the four propellers T_1, T_2, T_3 and T_4, then force 'F' (thrust) is directly proportional to w^2 (Force α w^2) [12-14].

3. EXPERIMENTAL WORK

The schematic diagram of quadcopter system has shown in Figure. 2. Which consists of mechanical part, flight controller, electronics speed controller and 4G communication module.

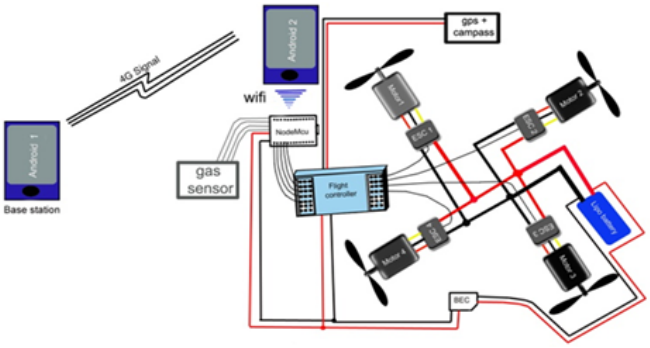

Fig.2. *Show the schematic diagram of quadcopter*

Designing and developing of all mechanical parts of Quadcopter in which F450 Quadcopter frame has been used in this project which has four arms on which 1000KV brushless motor is connected. Where KV is constant that is equal to rpm/volt. 1045 propeller is mounted with each motor which convert rotation of the brushless motor into an upward thrust. The upward thrust is directly proportional to the rotation of the motors. The speeds of brushless motors are controlled by 30A Electronic speed controller (ESC) according to the command received from the APM 2.8 flight controller. Neo-7m GPS+COMPASS module has also been used with flight controller to introduce different modes of function during the flight such as return to launch (RTL), acro, auto mode and position hold mode etc. A 11.1V, 5.2A Lithium Polymer battery has been used to power to all the circuitry, and motors of the quadcopter. A 4G based communication module has been introduced in this quadcopter which gives freedom to control quadcopter from any location where 4G network is available. An android cell phone has been used in Quadcopter for

providing video streaming, and communication between flight controller and base station. This cell phone is connected with flight controller via Nodemcu using wifi network. In base station another cell phone is utilized to provide control which has graphical user interface in blynk software. Base station cell phone works in same manner as that of wireless remote act as 4G transmitter. 4G recevier designed consisting of Nodemcu, output pins and a USB port/mobile internet. USB port has an alternative way of connecting internet connection with Nodemcu by using USB 3G/4G dongle as shown in Figure. 3. 4G transmitter having different types of control options such as thrust, pitch, yaw, roll and modes of flight.

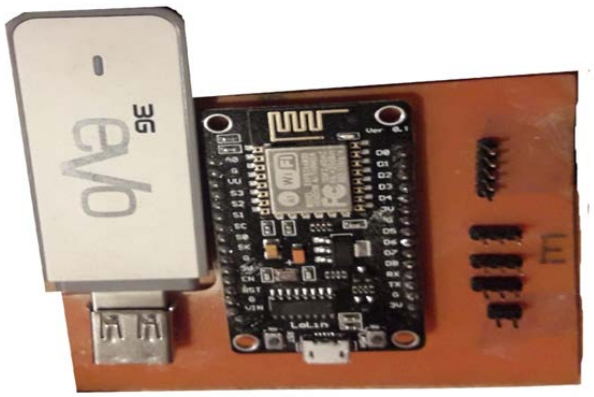

Fig.3. PCB designed of Nodemcu with USB port works as 4G receiver module

4G Communication Module

In this research two android mobile phones have been used as a transceiver communication module in which one android phone is connected with flight controller via Nodemcu and another android cell phone is on the base station which is connected through 4G to establish communication between flight controller and base station. The graphical user interface (GUI) of quadcopter control is developed in blynk software as shown in Figure. 4.

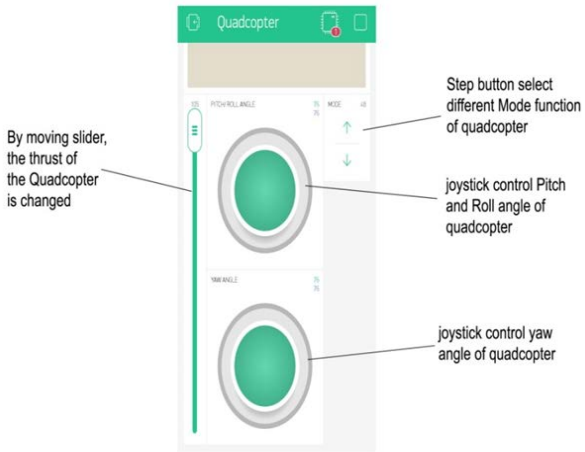

Fig.4. *Shows android mobile with blynk software*

In GUI widgets are used for different function such as slider is used for thrust control, joystick for pitch, roll and yaw angle and step button is used to select different modes of function for quadcopter. Each widget has a parameter that can be changed to set the desired PWM signal on the output of Nodemcu. Nodemcu is also known as Node microcontroller that supports wifi connectivity and is programmed by using standard computer programming. Nodemcu has several general purpose input/output pins in which 5 pins (D0-D4) are connected with the corresponding input of the flight controller for different function where D0 is assigned for Pitch angle control, D1 is assigned for Roll angle control, D2 is assigned for thrust (upward force), D3 for Yaw angle and D4 is assigned for different mode function of the quadcopter. As we found in the oscilloscope that the desired PWM signal for input of the flight controller has frequency of 50Htz and Duty cycle is to be from 20% to 25%. 20% Duty cycle represents minimum value whereas 25% Duty cycle represents maximum value as shown in Fig. 5,which means that if the slider widget is at minimum state, then pulse width of the signal is 20% and the rotation of the four brushless motors has minimum or zero speed which provide zero or minimum thrust (upward force) to the quadcopter. As the slider is moved toward maximum value, then pulse width of duty cycle will be increasing from 20% and thrust of the quadcopter will also be increasing by increasing the speed of the motors. When the slider reaches to its maximum state then duty cycle of PWM signal is 25% and provides full thrust (upward force) to the quadcopter to takeoff. Similarly same parameters are set for pitch angle, roll angle and yaw angle of the quadcopter. Android mobile with blynk application and duty cycle of PWM signal has shown in Figure. 5.

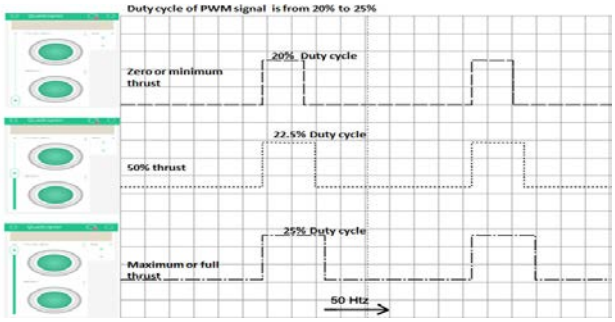

Fig.5. *Graph shows pulse width of the signal change from 20% to 25% by moving the slider*

4. RESULT AND DISCUSSION

Implementation of 4G communication in quadcopter has been done through which we can control the quadcopter from any location where 4G network is available. One android cell phone is the handheld user's mobile in which blynk software is installed and acts as a base station controller whereas another android cell phone is connected with the quadcopter frame that has two functions first function is to provide 4G communication between base station and flight controller and second function is to utilize its camera for live video streaming through which we can see the dynamics of the

quadcopter on the base station. Figure. 6 shows the quadcopter is to be controlled from the ground station.

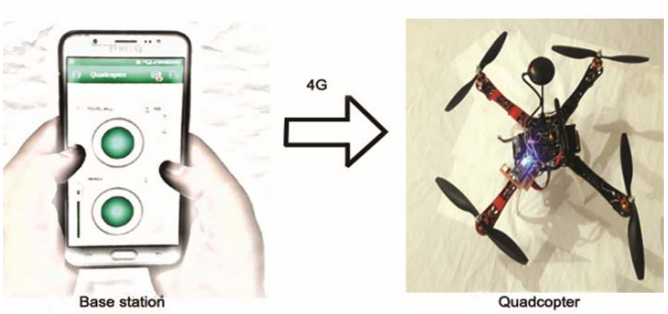

Fig.6. *Shows quadcopter controlled from base station*

Mission Planned

During experiment automatic mission has successfully been performed by selecting an AUTO mode in different flight modes then quadcopter has followed the preplanned path by using GPS module and servo gripper has also been connected with the flight controller for deliver and drop application. The path is defined and loaded from the mission planner software into the flight controller via personal computer. The following path has been followed by the quadcopter.

- Initially the quadcopter grabbed the ball with the help of servo gripper and took off vertically from the home position until attained 10 meter height.
- When the quadcopter attained its maximum height then it faced and moved toward the preplanned path (waypoint).
- When it reached to the maximum horizontal distance that is 500m from home position and reached to position 1 and then it produced yaw angle and moved toward position 2 and stayed over there for 6 second defined in the preplanned mission.
- After 6 second it landed and then dropped the ball at position 2.
- After dropping the ball at position 2 then it's taken off again and return to home position and landed at the same position from where it has been taken off at the beginning.

Path followed by quadcopter defined in mission planned has shown in the following Figure. 7.

Fig.7. *Show the path defined for quadcopter mission in mission planner software*

5. CONCLUSION

The development in the quadcopter facilitates the people that they can control the quadcopter from any region without fears of range limitation and it also help to send the quadcopter to those area where there is a security threat for human being and the events occurring in those areas can be seen through mobile or laptop screen using 4G network. It also helps to accomplish the auto mission with the help of GPS module from any region of the world just by changing the flight mode from stabilized to AUTO mode via GUI. It also helps the people to delivers and drop material application with the help of servo gripper.

ACKNOWLEDGEMENTS

Authors are really thankful to Physics Department University of Balochistan faculty for their hard work while making a long range Quadcopter and for arranging the stuffs required for its designing.

REFRENCES

[1]. Thu, K. M., & Gavrilov, A. I. (2017). Designing and Modeling of Quadcopter Control System Using L1 Adaptive Control. *Procedia Computer Science*, vol. *103* , p. 528-535.

[2]. Rajpoot, A. S., Gadani, N., &Kalathia, S. (2016). Development of Arduino Based Quadcopter. *International Advanced Research* Journal *in Science, Engineering and Technology*, vol. *3* no. 6.

[3]. Ononiwu, G., Onojo, O., Ozioko, O., &Nosiri, O. (2016). Quadcopter Design for Payload Delivery. *Journal of Computer and Communications*, *vol. 4, no. 10.*

[4]. Khan, M. (2014). Quadcopter Flight Dynamics. *International Journal of Science and Technology Research*, vol. 3, no. 8 p .130-135.

[5]. Pottams, A. J., Harikrishnan, V., Sankar, R., Raveendran, B., & Warier, S. R. Student, Department of Applied Electronics & Instrumentation, Rajagiri School of Engineering & Technology, kakkanad1 Faculty, Department of Applied Electronics & Instrumentation, Rajagiri School of Engineering & Technology, kakkanad2 (2016), QUADCOPTER, vol.7, no 11.

[6]. Wang, P., Man, Z., Cao, Z., Zheng, J., & Zhao, Y. (2016, November). Dynamics modelling and linear control of quadcopter. In *Advanced Mechatronic Systems (ICAMechS), 2016 International Conference* IEEE, p. 498-503.

[7]. Huynh, M. Q., Zhao, W., &Xie, L. (2014, December). L 1 adaptive control for quadcopter: Design and implementation. In *Control Automation Robotics & Vision (ICARCV), 2014 13th International Conference* IEEE p. 1496-1501..

[8]. Almurib, H. A., Nathan, P. T., & Kumar, T. N. (2011, September). Control and path planning of quadrotor aerial vehicles for search and rescue. In *SICE Annual Conference (SICE), 2011 Proceedings* IEEE p. 700-705.

[9]. Mahen, M. A., Anirudh, S., Naik, A., Chethana, H. D., & Shashank, A. C. (2014). Design and development of amphibious quadcopter. *International Journal of Mechanical and Production Engineering*, *2*(7), vol. 2, no. 7, p. 30-34.

[10]. Junior, J. C. V., De Paula, J. C., Leandro, G. V., &Bonfim, M. C. (2013). Stability control of a quad-rotor using a PID controller. *Brazilian Journal of Instrumentation and Control*, *vol.1, no.1, p.* 15-20.

[11]. Narkar, S., Kore, S., Jamgekar, R., & Doiphode, S. DTMF based Hybrid Robot for Air and Land.

[12]. Anand, S. S., & Mathiyazaghan, R. (2016). Design and Fabrication of Voice Controlled Unmanned Aerial Vehicle. *IAES International Journal of Robotics and Automation (IJRA)*, vol.5, no.3, p. 205-212.

[13]. Achtelik, M., Zhang, T., Kuhnlenz, K., & Buss, M. (2009, August). Visual tracking and control of a quadcopter using a stereo camera system and inertial sensors. In *Mechatronics and automation, 2009. icma 2009. international conference* IEEE, p. 2863-2869.

[14]. Argentim, L. M., Rezende, W. C., Santos, P. E., & Aguiar, R. A. (2013, May). PID, LQR and LQR-PID on a quadcopter platform. In *Informatics, Electronics & Vision (ICIEV), 2013 International Conference* IEEE, *p*. 2863-2869.

Techno-Science
Scientific Journal of Mehmet Akif Ersoy University
www.dergipark.gov.tr/sjmakeu

DEHYDRATION OF VEGETABLES BY USING INDIRECT SOLAR DRYER

Younas KHAN[1*], Jafar Khan KASI[1], Ajab Khan KASI[1]

[1] *Department of Physics, University of Balochistan, Quetta, Pakistan*

HIGHLIGHTS

- Indirect solar dryer is designed to dry vegetables such as tomatoes, eggplant, onion and mint leaves.
- Indirect solar dryer is designed with low cast and easy to process.
- Indirect solar dryer provide close atmosphere for the agricultural products.
- It has temperature controlled system in the range of 50-60^{o}C, avoiding the high temperature which may damage the quality of the products.

GRAPHICAL ABSTRACT

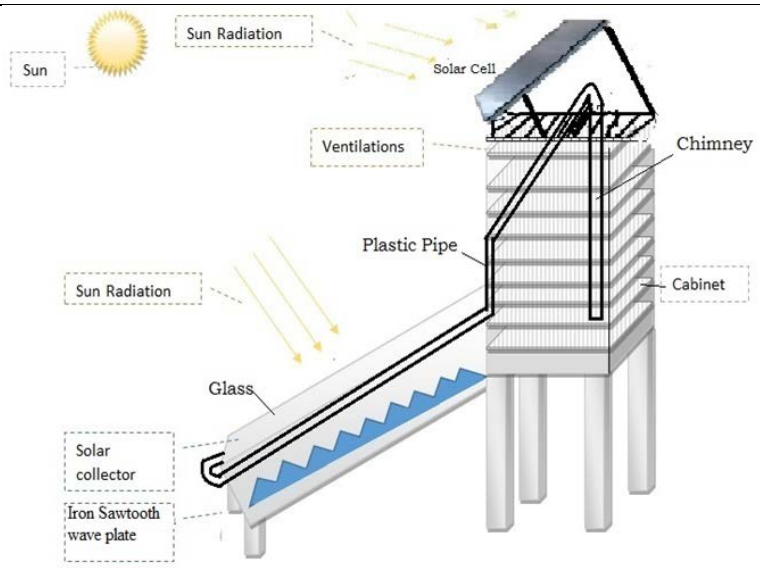

ARTICLE INFO

Article History

Received	:	21/09/2018
Revised	:	30/09/2018
Accepted	:	30/09/2018
Available online	:	30/09/2018

Keywords

Low cost dryer
Saw tooth wave absorber plate
Uniform heated air dryer
Tomatoes
Mint leaves
Eggplant
Onion

ABSTRACT

The temperature controlled indirect solar dryer is designed in Quetta by using simple available stuffs in the market to dry the agricultural products for its longer shelf life. The dryer consists of drying cabinet, solar cell, electrical fan and collector. Inside the cabinet there are four trays at equally distance from each other, each tray receive uniformly heated air from the collector to dry the agricultural product. During the drying process temperature and relative humidity inside the cabinet is measured with help of digital hygrometer. Tomatoes, mint leaves, eggplant and onion were dried in newly low cost designed dryer. The drying time, color and quality of these products are compared with open sun drying. The result shows that the product dried in the newly dryer is good in quality and dry faster than open sun drying method. The drying occurs in falling rate period. Uniformity of the dryer in each tray was also checked by placing vegetable slices of same size and weight in each tray, the drying time for each tray was same. By increasing the size of vegetable slices increase the drying time, result also shows that increasing in drying air temperature also increase the drying time.

1. INTRODUCTION

Drying is a process to remove the water from the agricultural products in order to increase its shelf life [1]. Drying is one of the oldest methods to save the food from spoilage and store it for longer period of time without use of refrigerator [2]. The drying of agricultural products is done for two purposes; the first is to stop the growth of micro-organism and second is to store it for longer period of time [3]. Drying reduces space for storage, lighter the

* Corresponding Author: younaskhankasi@gmail.com

To cite this article: Khan, Y., Kası, J.K., Kası, A.K. (2018). Dehydration of vegetables by using indirect solar dryer. *Techno-Science* vol. 1, no. 1 p. 22-28.

weight, make it easy for the transport of the agricultural product and make sure its presence throughout the year [4]. Open sun drying is traditional method to dry the agricultural products. This method is practice in many developing countries because the energy required in this process is free, renewable, non-polluted and abundant in most of the environments [5]. As this method is cheap and easy to process but it contains some drawback such as microbial attack, dust, rain and insects which damage the products [6]. In this method agricultural product is placed in open ground on which sunlight directly exposure on the product to dry it, this damage the colour and quality of the product [6]. The products dried in traditional method are not acceptable in standard market which is economic loss of the country [7]. To overcome these problems, the agricultural products should be dried in solar dyer, the solar dryer provide close atmosphere for dryer process to save the product from microbial attack, rain, dust, and insects in order to improve the quality of the products. Different researcher designed different types of dryer.

Azad explained the two modes (mixed + indirect) dryer to dry the grapes in five days, moisture from the grapes is reduced from 81.1% to 36.7% [8]. Amer et al., designed hybrid dryer to dry banana from moisture content 82 to 18% [9]. Musembi designed indirect natural convection solar dryer to dry apple from moisture content 86% to 8.12% [10]. Different types of dryers have been used for drying vegetable products, Tunnel solar dryer which consist of a transparent plastic sheet, two DC fan and flat plate collector which is connected in series to dry pineapple from moisture content 87.32% (wet basis) to 14.13% (wet basis) in 3 days [11]. Chen et al. designed close type solar dryer to dry lemon slices [12]. The small size dryer which consists of biomass burner to provide heat at night time was designed by Bena and Fuller to dry fruits and vegetables [13]. The aim of this research is to study and design low cost and easy process dryer, which can provide close atmosphere to save the product from microbial attack, dust, rain and insects. For controlled temperature (from 50˚C to 60˚C) an automatic system, is installed in the dryer which maintains the temperature throughout drying cabinet to dry short life agricultural products for longer period of time.

2. METHODS

2.1. Indirect Solar Dryer

Indirect solar dryer is designed in Quetta from local stuffs available in the market during the year of 2018. The designed dryer is so simple that it can be constructed by farmer for dying agricultural products. The dryer consists of solar cell, cabinet, and collector. The schematic diagram of solar dryer is shown in Figure 1.

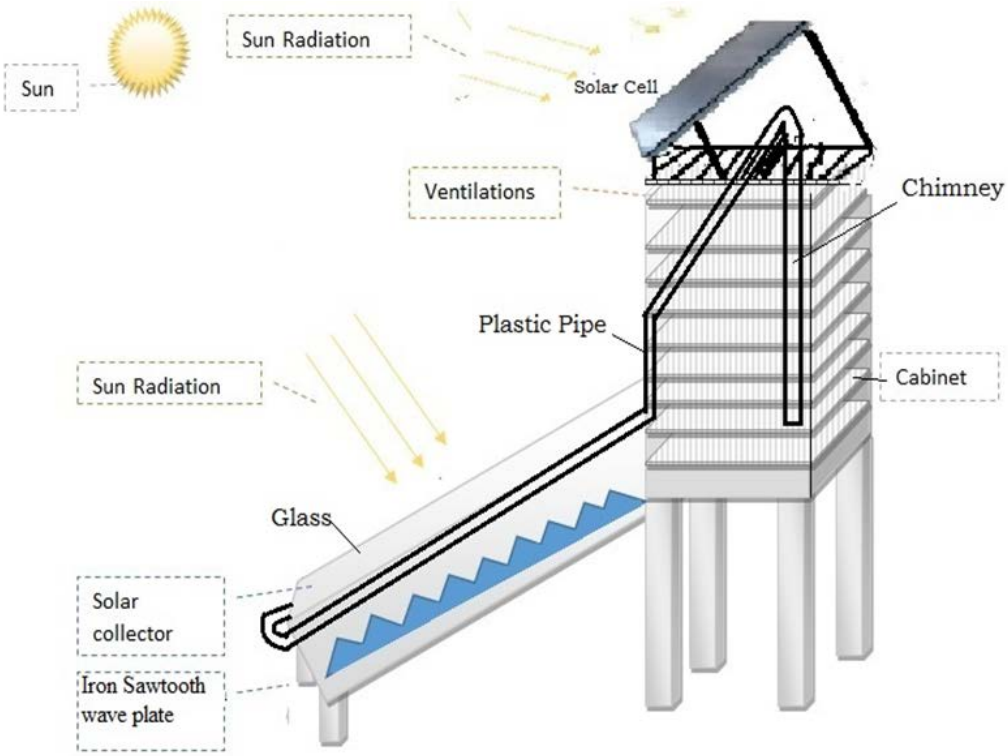

Fig. 1. *Indirect solar dryer*

2.2. Solar Cell

The dimension of solar cell is 53x76 (cm). The maximum power of solar cell is 50W; maximum power voltage (V_{mp}) is 18.2V and its maximum power current (I_{mp}) is 2.7A. The purpose of solar cell is to run the electrical fan connected with designed dryer.

2.3. Collector

Collector consists of electrical fan, absorber plate and transparent glass. The dimension of collector is 2ft in width and 4ft in length and the dimension of the glass is (0.49x121.92 (cm)). At the base of collector there is mat mash (net) which is the path for entering the fresh air from surrounding. The absorber plate of length 3ft is in the form of sawtooth waves which is placed in collector. The absorber plate is black painted to absorb more sun light. The purpose of sawtooth wave form of absorber plate is to increase the surface area of the collector. When fresh air from atmosphere enters through a mat which is at base of collector, the molecules have more contact time with sawtooth wave form of absorber plate and increase the heat energy of the air molecules. The heated air is forced in the cabinet by means of electrical fan. There are five electrical fans from which two are placed at the base of the collector and three are placed at the end of the collector. These electrical fans are run with the help of solar cell. The fans at the base are used to take air from the atmosphere and push it into the dryer, which decreases the temperature of the dryer up to 3℃. Where three fans at the end of collector forces the heated air in the drying cabinet. At the base of the collector there are two small doors which are closed at night time avoiding the air entry from surrounding into the dryer.

2.4. Drying Cabinet

The dimension of drying cabinet is 3ft in height and 2ft in width was constructed from plywood which is light in weight. This plywood is supported by frame of massive wood. The cabinet is at height 2ft from the surface of earth by means of four legs. The cabinet of the dryer is made from plywood, beside of it three sides wall and top side of the cabinet is also made from Iron sheet in order to increase the temperature of the cabinet. The iron sheets are joined together in such a way that there is no leakage of air from it. The back side of iron sheet (collector side) has 4 holes of 4cm diameter at left side and 4 holes of 4cm diameter at right side. The holes of both sides are parallel to each other. Pipes of dimension (2.5x51cmx4.1 (cm)) are fixed in these holes; each pipe has equal number of holes except the bottom pipe which has 4 extra holes. The number of pipe in the cabinet is eight, four from left side and four from right side. These pipes are fixed in the holes of iron sheet such that they are parallel to each other. The cabinet have four trays which are made from mat mash and supported by frame of wood, these trays have dimension (19.7x20.2 (cm)) are placed on the pipes. The heated air from the collector enters in the pipes, from the holes of the pipes it comes in the cabinet. These heated air take out moisture from the agricultural product which were placed on the tray and comes out from the holes which is at the top side of iron sheet and from here it cannot escape in the atmosphere because at the top of iron sheet there is plywood roof, so the moisture air is recirculated from the side of iron sheet then come out from the chimney. This recirculation of air from the sides of the conductor heats the iron sheet and increases the temperature of the cabinet. The air which comes out from the chimney is again entering at the base of the collector with the help of plastic pipe which helps to increase the temperature up to 2℃.

3. EXPERIMENTAL

In the designed dryer tomatoes, mint leaves and apricots were dried, the drying time and quality of the dried product is compared with product which is dried in open sun method.

3.1. Drying of Tomatoes

Fresh tomatoes were purchased from local market. Before slicing the tomatoes, it was washed with clean water and dried with soft piece of cloth. After cleaning and drying the tomatoes was cut into slices with sharp knife. About 30g of sliced tomatoes having thickness 5mm were placed in the dryer. Before starting the experiment the dryer was run up to one hour to gain its momentum. The experiment was carried out from 10.00 AM in the month of August. The 30g of same size tomatoes were placed on net above the surface from earth under open sun light. The weight loss of tomatoes slices was measured after every one hour with digital physical balance (±1g) heaving maximum capacity 7kg. The moisture content of tomatoes slices was removed up to 93.33% (wb).

3.2. Mint Leaves

Second vegetable for drying was mint. The fresh mint leaves were purchased from the local market, were washed dried. After washing the mint leaves, about 15g of mint leaves were placed in dryer as a drying sample. The mint leaves is separated from its branches. The same quantity of mint leaves were placed in net which is above from the ground under open sun light. The weight loss of mint leaves was measured with the help physical balance after every 30min. The initial moisture content of mint leaves was 80% (wb).

3.3. Eggplant

Fresh eggplants were purchase from local market of Quetta. The eggplant is washed and dried from soft clean cloth then placed at room temperature for 15min. After that eggplant is cut into slices of 5.5mm, 55g of eggplant was placed into the dryer. The weight loss of the eggplant slices were measured with digital physical balance after every one hour.

3.4. Onion

Fresh onions were purchased from the local market. The onion is cut into its slices of 3mm, and 33g of onion were placed into the dryer. The weight loss of onion was measured after every one hour.

3.5. Uniformity of the Dryer

To check the uniformity of the dryer the tomatoes slices of size 5mm having weight 30g were placed in four trays of the dryer. The weight loss of the tomatoes was measured after every one hour with the help of digital physical balance.

3.6. Effect of Temperature on Drying Process

It was observed that drying air temperature greatly affect the drying time. The 30g of tomatoes slices of size 5mm was placed in the solar dryer, the temperature inside the dryer is in the range of 45-50℃. This temperature was less as usual temperature range of the dryer because of cloudy day. The weight of the tomatoes was measured after every one hour by using digital balance. The drying process was continued until there is no change in weight of tomatoes slices observed. The same size and weight of tomatoes slices were placed in solar dryer having temperature in the range of 50–60℃ in shining day. This temperature is the maximum range temperature of the dryer. The change in weight is measured after every hour.

3.7. Temperature and Relative humidity

The range of temperature inside the dryer is 50 to 60℃ and relative humidity is 10% which is measured with the help of digital hygrometer. Where the ambient temperature range is 35 to 38℃ and relative humidity is 10%. At night ambient temperature is in the range of 20 to 32℃ and range of relative humidity is 35 to 70%.

3.8. Moisture Content

The moisture content of the drying products was determined by using formula.

$$MC = \frac{W_i - W_{ab}}{W_i} (\%\ \text{wb}) \quad (1)$$

Where MC is moisture content, W_i is initial weight and W_{ab} is bone-dry weight. The equilibrium moisture content was found out when there is no further changes in weight of the product. Wet basis (wb) means (g of water/g of moist sample).

3.9. Moisture Ratio

The moisture ratio can be calculated by using formula:

$$MR = \frac{M_t - M_e}{M_i - M_e} \quad (2)$$

Where MR is moisture ratio, M_e is equilibrium moisture content of product (g water/ g of moist solid). The value of M_e is very small relatively small compared to M_t or M_i so M_e is consider to be zero Diamante and Munro [14].

4. RESULT AND DISCUSSION

The drying behaviour of agricultural product depends on drying air temperature and relative humidity. The increase in drying air temperature increases the drying rate and decrease the drying time. The increase in humidity slows the drying rate and increase the drying time. This statement was confirmed by several authors [15-18]. The dryer provide close atmosphere for dying the agricultural products and protects the product from microbial attacks, rain, dust and insects. The dryer also protect the product from humidity, the area which have high humidity then drying the agricultural products in open sun drying increase the drying time because the humid air is unable to take out moisture from the products. In such area the dryer is used to speed up the drying process.

The drying behaviour of tomatoes slices in dryer and open sun method is shown in Figure. 2. The graph shows that moisture content reach to its equilibrium position faster than traditional method. The graph shows that there is not constant rate drying period while drying occurs in falling rate period. In falling rate period drying rate decrease continuously with decrease in moisture ratio. To check the quality of the dried product, the dried product is shown to the different experts. The result obtain from the experts shows that the quality of the

tomatoes slices dried in dryer is good than open sun drying which contain dust particle.

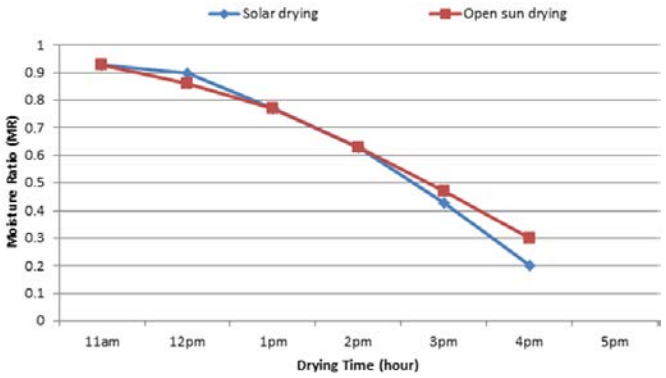

Fig. 2. *Drying behaviour of tomatoes in Solar Dryer vs Open sun*

By increasing the size of the tomatoes slices effect the drying time, increase in the size of thickness increase the drying time as shown in Figure 3. This result was confirmed by several authors in their paper [19-21].

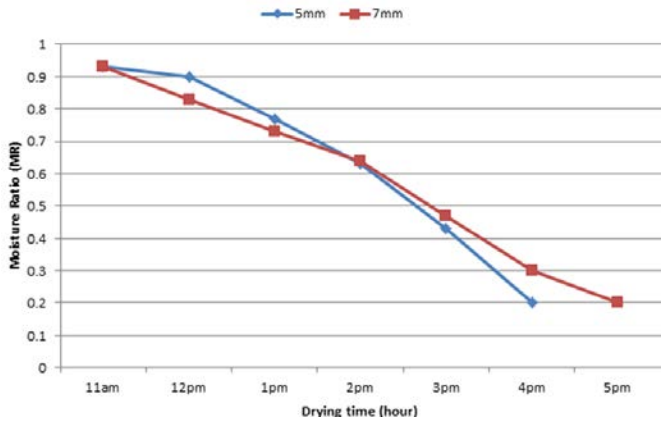

Fig,3. *Size effect of tomatoes on drying time*

The uniformity of the dryer is shown in Figure 4. The graph shows that drying time is approximately same in each tray and moisture content reach to its equilibrium position in the same time.

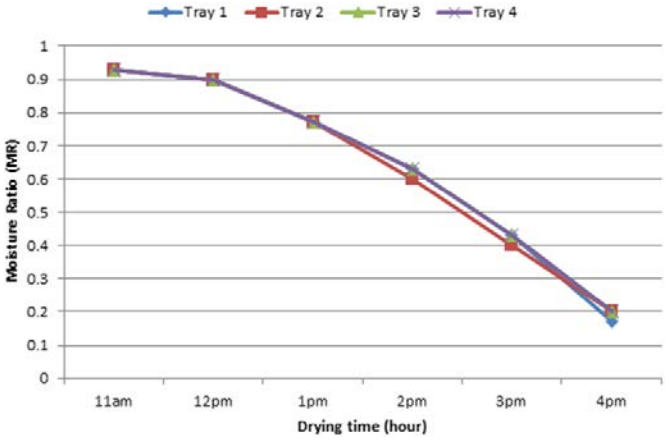

Fig. 4. *Uniformity of the dryer*

The Figure 5 shows that drying process of mint leaves. The drying of mint leaves occur in falling rate period. The graph shows that the drying process is fast in newly designed dryer as compare to open sun drying.

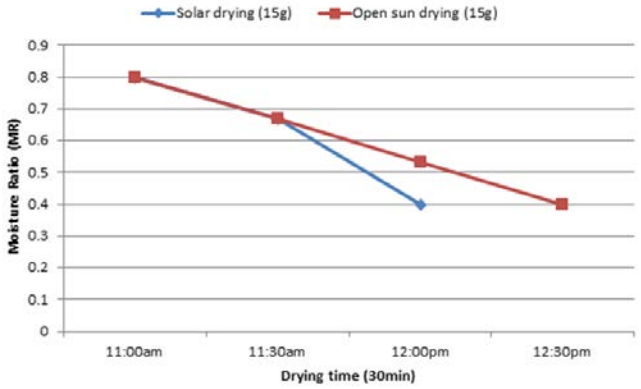

Fig. 5. *Drying behaviour of mint leaves in Solar Dryer vs Open Sun*

The drying process depends on drying air temperature, by increasing the drying air temperature increase the drying rate. The Figure 6 shows the result of tomatoes of same size and weight but different temperature range. The temperature ranges in drying process of tomatoes slices of same size are 45-50°C and 50-60°C. It shows that increase in temperature increase the rate of drying process.

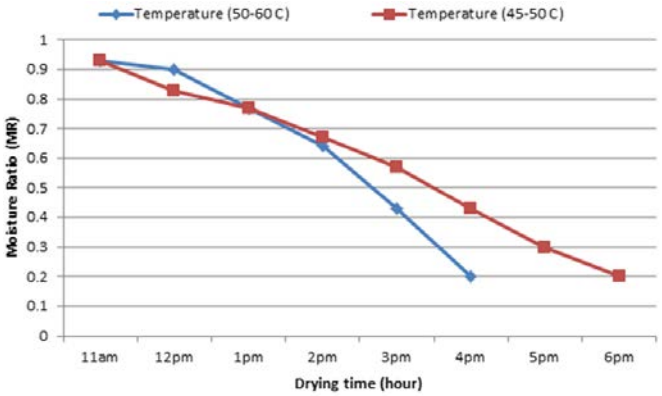

Fig. 6. *Temperature effect on drying time*

Figure 7 and 8, shows the drying behaviour of eggplants and onions. The drying behaviour of eggplant and onion in designed solar dyer were compare with open sun process. The drying process is fast in dryer than open sun. The drying occur in falling rate period not in constant rate.

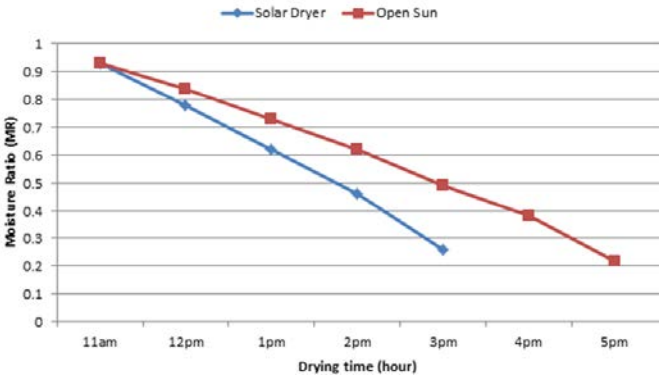

Fig. 7. *Drying behaviour of Eggplant in Solar Dryer vs Open Sun*

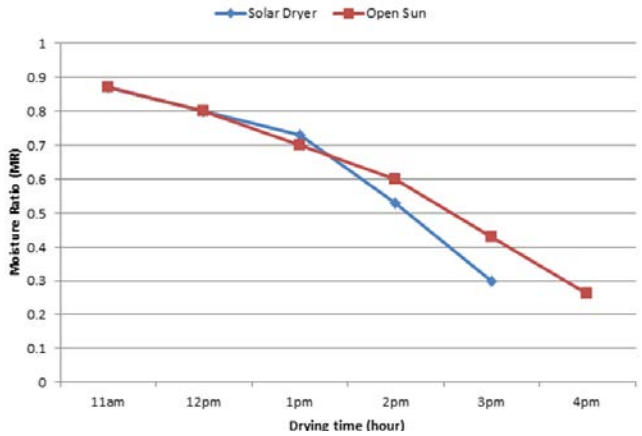

Fig. 8. *Drying behaviour of onion in solar dryer vs open sun*

5. CONCLUSION

The newly designed dryer was used to dry the tomatoes, mint leaves, eggplant and onion. The designed dryer provides close atmosphere to dry the product in order to protect it from microbial attacks, dust, rain and insects. The drying of these products occurs in falling rate period. Drying time of the dried products in the designed dryer is less than open sun drying and quality of the product in dryer is also good than open sun method. It was observed that increase in drying air temperature increase the drying rate and decrease the drying time. The total cost of the dryer is low so it reduced the cost of drying product.

ACKNOWLEDGEMENTS

Authors are really thankful to Mr. Yaqoob Kasi and Mr. Yousaf Kasi for their hard work while helping to design the newly low cost dryer and for arranging the stuffs required for its designing.

REFRENCES

[1]. Sarsilmaz, C., Yildiz, C., & Pehlivan, D. (2000). Drying of apricots in a rotary column cylindrical dryer (RCCD) supported with solar energy. *Renewable Energy*, vol. 21, no. 2 p. 117-127.

[2]. Demiray, E., & Tulek, Y. (2012). Thin-layer drying of tomato (Lycopersicum esculentum Mill. cv. Rio Grande) slices in a convective hot air dryer. *Heat and Mass Transfer*, vol. 48, no. 5 p. 841-847.

[3]. Ashtiani, S. H. M., Salarikia, A., & Golzarian, M. R. (2017). Analyzing drying characteristics and modeling of thin layers of peppermint leaves under hot-air and infrared treatments. *Information Processing in Agriculture*, vol. 4, no. 2 p. 128-139

[4]. Al-Juamily, K. E., Khalifa, A. J. N., & Yassen, T. A. (2007). Testing of the performance of a fruit and vegetable solar drying system in Iraq. *Desalination*, vol. 209, no. 1-3 p. 163-170.

[5]. Bahloul, N., Boudhrioua, N., Kouhila, M., & Kechaou, N. (2009). Effect of convective solar drying on colour, total phenols and radical scavenging activity of olive leaves (Olea europaea L.). *International journal of food science & technology*, vol. 44, no. 12 p. 2561-2567.

[6]. Doymaz, I. (2006). Thin-layer drying behaviour of mint leaves. *Journal of Food Engineering*, vol. 74, no. 3 p. 370-375.

[7]. Tiris, C., Tiris, M., & Dincer, I. (1996). Experiments on a new small-scale solar dryer. *Applied Thermal Engineering*, vol. 16, no. 2 p. 183-187.

[8]. Azad, E. (2008). Design and experimental study of solar agricultural dryer for rural area. *Livestock Research for Rural Development*, vol. 20, no. 9 p. 2008

[9]. Amer, B. M. A., Hossain, M. A., & Gottschalk, K. (2010). Design and performance evaluation of a new hybrid solar dryer for banana. *Energy conversion and management*, vol. 51, no. 4 p. 813-820.

[10]. Musembi, M. N., Kiptoo, K. S., & Yuichi, N. (2016). Design and Analysis of Solar Dryer for Mid-Latitude Region. *Energy Procedia*, vol. 100, no. 1 p. 98-110.

[11]. Bala, B. K., Mondol, M. R. A., Biswas, B. K., Chowdury, B. D., & Janjai, S. (2003). Solar drying of pineapple using solar tunnel drier. *Renewable Energy*, vol. 28, no. 2 p. 183-190.

[12]. Chen, H. H., Hernandez, C. E., & Huang, T. C. (2005). A study of the drying effect on lemon slices using a closed-type solar dryer. *Solar Energy*, vol. 78, no. 1 p. 97-103.

[13]. Bena, B., & Fuller, R. J. (2002). Natural convection solar dryer with biomass back-up heater. *Solar energy*, vol. 72, no. 1 p. 75-83.

[14]. Diamante, L. M., & Munro, P. A. (1993). Mathematical modelling of the thin layer solar drying of sweet potato slices. *Solar energy*, vol. 51, no. 4 p. 271-276.

[15]. Demiray, E., & Tulek, Y. (2012). Thin-layer drying of tomato (Lycopersicum esculentum Mill. cv. Rio Grande) slices in a convective hot air dryer. *Heat and Mass Transfer*, vol. 48, no. 5 p. 841-847.

[16]. Celma, A. R., Cuadros, F., & López-Rodríguez, F. (2012). Convective drying characteristics of sludge from treatment plants in tomato processing industries. *Food and Bioproducts Processing*, vol. 90, no. 2 p. 224-234.

[17]. Movagharnejad, K., & Nikzad, M. (2007). Modeling of tomato drying using artificial neural network. *Computers and electronics in agriculture*, vol. 59, no. 1-2 p. 78-85.

[18]. Ringeisen, B., Barrett, D. M., & Stroeve, P. (2014). Concentrated solar drying of tomatoes. *Energy for sustainable development*, vol. 19, no. 1 p. 47-55.

[19]. Khazaei, J., Chegini, G. R., & Bakhshiani, M. (2008). A novel alternative method for modeling the effects of air temperature

and slice thickness on quality and drying kinetics of tomato slices: superposition technique. *Drying Technology*, vol. 26, no. 6 p. 759-775.

[20]. Sadin, R., Chegini, G. R., & Sadin, H. (2014). The effect of temperature and slice thickness on drying kinetics tomato in the infrared dryer. *Heat and Mass Transfer*, vol. 50, no. 4 p. 501-507.

[21]. Rajkumar, P., Kulanthaisami, S., Raghavan, G. S. V., Gariépy, Y., & Orsat, V. (2007). Drying kinetics of tomato slices in vacuum assisted solar and open sun drying methods. *Drying Technology*, vol. 25, no. 7-8 p. 1349-1357.

Techno-Science

Scientific Journal of Mehmet Akif Ersoy University

www.dergipark.gov.tr/sjmakeu

This page intentionally left blank

This page intentionally left blank

This page intentionally left blank